Capability of pulse-limited satellite radar altimetry to monitor inland water bodies

Master Thesis

Shirzad Roohi

Stuttgart, May 2015

Supervisor: Prof. Dr.-Ing. Nico Sneeuw
University of Stuttgart

Erklärung der Urheberschaft

Ich erkläre hiermit an Eides statt, dass ich die vorliegende Arbeit ohne Hilfe Dritter und ohne Benutzung anderer als der angegebenen Hilfsmittel angefertigt habe; die aus fremden Quellen direkt oder indirekt übernommenen Gedanken sind als solche kenntlich gemacht. Die Arbeit wurde bisher in gleicher oder ähnlicher Form in keiner anderen Prüfungsbehörde vorgelegt und auch noch nicht veröffentlicht.

Ort, Datum   Unterschrift

Summary

Pulse-limited satellite altimeters were originally designed for oceanographic observations but they have been extended to monitor inland water bodies. So far, studying water level variations of inland water bodies, e.g. lakes, has been a challenge for this type of altimetry in terms of data quality. The returned altimetry waveforms can be seriously contaminated by topography and environmental error sources. Retracking is an effective method against this contamination to improve the accuracy of range measurement and, consequently, to determine more accurate water level. In addition, the design of an optimal retracking algorithm appropriate for a specific inland water body is very important in this respect.

In this study we processed 1 Hz Geophysical Data Record (GDR) of Envisat RA2 altimetry data by on-board tracker and retrackers. We also analyzed 18 Hz data of this mission, i.e. Sensor Geophysical Data record (SGDR), with respective different retrackers. First we processed GDR data to determine water level variations from ALL, MEDIAN and MEAN values of water level in each satellite pass over an inland water body. In this step we analyzed to find the best on-board tracker and retrackers. In the next step, the whole waveform, called full-waveform, was processed to estimate retracked water level variations using OCOG, Threshold and β-parameter retrackers. Then we assumed that the reflecting surface inside the radar foot print is a complex surface with different responses. Therefore a given waveform was considered as a combination of a number of small waveforms, called sub-waveform. Each sub-waveform was processed by all of the mentioned retrackers to determine water level variations.

The largest salt lake in the middle east, Urmia lake, has been selected as a testing area in this study. We found out that between on-board tracker and on-board retrackers the MEDIAN values, processed by ice-1 retracker, provide the most accurate water level variations. Finally the result of different retracked water level were compared with ice-1 retrackers, and with available in-situ gauge data. Our analysis shows that retracking on the sub-waveform outperforms the retracking on the full-waveform. The minimum RMS, 18 cm, was achieved by sub-waveform, retracked by Threshold 50% algorithm. Therefore sub-waveform retacked by threshold 50% is the best retracking scenario to retrieve the water level variations of Urmia lake.

Contents

List of Figures

List of Tables

Chapter 1

Introduction

A regional inland water body is the habitat for diverse biological communities such as birds and other creatures. Many human activities in different fields, e.g. fishery, agriculture, urban and industrial water purification and flood management, rely on the inland water. These activities change the quantity and quality of water that can be a potential threat not only for the ecosystem but also for the human life. Furthermore, because of water resource limitations climate change can exacerbate the water quantity reduction of inland water bodies.

An optimized water management for inland water bodies requires the knowledge of the surface water resource distributions and water level changes. Freshwater lakes, as easily accessible water resources, represent about 95% of surface freshwater on the Earth's surface that support water supply for wild life and human activities (Lee et al., 2010). Therefore we must know how the storage of these water bodies change and how they react to climate change and human activities. Hydrology, as a discipline dealing with the water cycle, is related to the resource, volume and distribution of water in the global and regional scale. Monitoring and modeling of water level variations and discharges, represent a basis for hydrology to develop and to manage regional water resources. Despite its important role, hydrology still depends on traditional and old measurement networks, in-situ gauge. In-situ gauge networks are not able to provide enough input data for hydrological models. Because the spatial distribution of these networks is not homogeneous around inland water bodies, especially in developing countries. It is difficult to install them in remote areas. They are vulnerable especially during the flood seasons and their maintenance, establishment and operation are expensive and difficult. Since installation of in-situ gauge networks follows national policy there is no unique database of their measurements to access openly. Particularly in boundary zones sharing these data would be very important. It would require an agreement between governments of different countries (Biancamaria et al., 2010). During the last 10–15 years the number of in-situ gauge stations has decreased in all of the world significantly (Shiklomanov et al., 2002) that is a great concern for the scientific community in detection of the impact of global change on the hydrological cycle. With these limitations, the hydrological model for water monitoring would not be complete if we have only in-situ gauge measurements.

Satellite radar altimetry helps us to partially overcome these limitations. It is a sophisticated and mature space-borne technology originally designed to measure ocean and sea surface height. With recent developments in the radar system of satellite altimetry missions like Envisat and CryoSat-2, radar altimetry has been extended to many other studies involving innovative applications to the inland water bodies. This technique provides water level measurements for most of the water bodies day and night in all weather conditions. It has revolutionized the ocean science with its unprecedented accuracy of several centimeters in determining

the sea surface height from space (Fu and Cazenave, 2001). Tseng et al. (2013) determined the sea surface height in coastal zones with RMS of 21 cm respect to in-situ gauge data. Over the Antarctic ocean Yang et al. (2012) obtained less than 10 cm of RMS in water level determination compared with tide gauge time series.

Even though altimeters provide accurate measurements of water level for oceans and large seas, over inland water bodies, e.g. lakes and rivers, their performance is limited in terms of spatial and temporal resolution as well as their accuracy in water level determination. Over the inland water bodies maybe the area inside the footprint of the radar is not purely water. Therefore the response of the radar pulse would be partially form none water surface that contaminates the measured waveform. This contamination reduces the accuracy of water level determination.

Waveform retracking techniques help us to increase the accuracy of water level monitoring for inland water bodies and to extend the application of satellite altimetry to monitor small inland water bodies. A comparison between in-situ hydrological data and retracked water level from TOPEX/POSEIDON in (Morris and Gill, 1994) showed very good performance of this mission over the Great lakes, the RMS of about 4 cm was obtained in this study. Hwang et al. (2005) analyzed data of this mission for different lakes in China. They found contaminated waveforms over these lakes and they mentioned it is necessary to retrack them. Guo et al. (2009) did waveform retracking using TOPEX/POSEIDON data over Hulun lake in the North of China. They indicated that waveform retracking techniques perform quite well in monitoring lake level and seasonal variations. In this study the maximum and minimum RMS with respect to the in-situ gauge data are about 25 cm and 10 cm for sub-waveform retracked by threshold algorithm. Lee et al. (2011) processed RA2 GDR data of Envisat satellite to determine water level of lakes Qinghai and Ngoring in China and lake Athabasca in Canada using on-board tracker and retrackers. Their result indicates that ice-1 retracker provides water level variation with a minimum RMS of 12 cm with respect to the in-situ gauge data for lake Athabasca. Over ice-covered lake like Qinghai, Tseng et al. (2013) demonstrated an RMS of less than 10 cm compared with in-situ gauge time series. Jain et al. (2015) investigated sea surface height changes in the Arctic region based on CryoSat-2 SAR waveform retracking. They retracked only the first detected sub-waveform with empirical retracking algorithms in summer and winter times. All retrackers have almost the same performance for summer and winter times. They obtained a minimum RMS of 3 cm for estimated sea surface anomaly using Offset Center Of Gravity (OCOG) retracker. In (Kleinherenbrink et al., 2014) the position of retracked gate was estimated from cross-correlation between observed waveform of CryoSat-2 SARIn mode and a generic simulated waveform. In this study, water level estimated from CryoSat-2 SARIn mode was validated against Jason-2 derived water level with an RMS of 30 cm for Nasser lake in Egypt.

Since there is no standard retracking algorithm to retrack the waveforms over all inland water bodies, in this study we do waveform retracking:

- to analyze the performance of different retracking algorithms

- to select the best retracking scenario to estimate water level variations

- to increase the number of valid observations

- to increase the quality of water level estimation

for a given inland water body.

To this end, we employed different retrackers to estimate water level variations with accuracy better than what is estimated by on-board tracker and on-board retrackers. We did full and sub-waveform retracking analysis in front of different retrackers, i.e. OCOG, Threshold and β-parameter, to find the optimized retracker algorithm for a specific inland water body.

In the second chapter we write about the principle of satellite radar altimetry. The area of study and data set are described in the third chapter. We process altimetry data with our methodology using on-board tracker and on-board retrackers to determine water level in chapter four. In this chapter we compare determined water level from ALL, MEDIAN and MEAN values of water level in each satellite over pass and select the most robust estimator for water level monitoring of the study area. Chapter five deals with waveform retracking algorithms. In this chapter we discuss the theory and mathematics as well as some assumptions behind these retracking techniques. We process SGDR data and compute retracked range correction, i.e. retracked range correction, in chapter six. These corrections are added to the ranges from GDR files for further process, e.g. to determine retracked water level variations. In this chapter we analyzed the result obtained from different retrackers to select the best retracker algorithm for water level monitoring of the study area.

Chapter 2

Satellite altimetry

Satellite radar altimeters were primarily designed to study variations in the water surface of open ocean and ice sheets (Fu and Cazenave, 2001). Today, due to advances in radar systems and data processing methodology, they provide accurate measurements over not only open ocean but also over inland water bodies, e.g. lakes and rivers. Innovative use of data has brought this opportunity to extend altimetry applications to different disciplines, e.g. climate change and crustal deformation of earth as well as hydrology. The main advantage is that radar altimeters sample the earth's surface day and night in all-weather conditions (Vignudelli et al., 2011). Thanks to their high accuracy, repeatability and stability, they have become an irreplaceable tool to address a wide variety of scientific questions from global ocean monitoring, long-term sea level rise, climate change to monitoring small lake level variations. Today there is increasing demand for satellite altimeter observations over the coastal zones and small inland water bodies. The radar system mounted on the satellite platform can observe monthly, seasonal and annual variations of different surfaces with respect to a specific reference frame to have a globally consistent uniform database. The spatial and temporal coverage of an altimeter depend on the satellite repeat orbit design. It is an important factor in monitoring water level variations. Dependent on the mission purpose usually an altimeter satellite is placed in a fixed repeat orbit. It's repeat cycle duration then governs the time resolution, whereas the inter-track spacing defines the spatial resolution.

2.1 Repeat orbit

A careful repeat orbit design plays an important role in sampling the water bodies from space. If the satellite mission focuses on inland hydrological applications, it must be able to monitor water bodies such as lakes and rivers with sufficient spatial and temporal resolution. A repeat orbit mode β/α occurs if the satellite performs β revolutions with respect to its ascending node in α nodal days. A nodal day is the time between two consecutive passages of a fixed earth meridian (Greenwich) over the satellite ascending node. β and α are co-prime integer numbers, i.e. they should not have a common factor. One can write $\beta/\alpha = I + N/\alpha$. I the integer part and N is fractional part. Geometrically the β/α ratio means commensurability, i.e. the satellite returns over the same point on its ground track after β revolutions and α nodal days. There are many perturbing force that affect on the satellite repeat orbit. Here we consider only the effect of the earth oblateness on the repeat orbit, called J_2 effect, that is the largest gravitational perturbing force. So we have following equations (Kaula, 1966):

$$\frac{\beta}{\alpha} = \frac{\dot{M} + \dot{\omega}}{\omega_e - \dot{\Omega}} = \frac{T_\Lambda}{T_u} \ , \tag{2.1}$$

Table 2.1: Satellite mission and operating characteristics of altimeters (http://www.aviso.altimetry.fr)

Altimeter	Launch	End	H (km)	Inclination	Band	Frequency (GHz)
Geosat	12 Mar 1985	Jan1990	800	108°	Ku	13.5
ERS-1	17 Juli 1991	Mar 2000	784	98°	Ku	13.8
Topex	10 Aug 1992	Jan 2006	1336	66°	Ku C	13.6 5.3
Poseidon	10 Aug 1992	Jan 2006	1336	66°	Ku	13.65
ERS-2	21 Apr 1995	Sep 2011	784	98°	Ku	13.8
GFO	10 Feb 1998	Sep 2008	800	108°	Ku	13.5
Jason-1	7 Dec 2001	Jul 2013	1336	66°	Ku C	13.6 5.3
Envisat	1 Mar 2002	May 2012	784	98°	Ku S	13.6 3.2
Jason-2	20 Jun 2008	Present	1336	66°	Ku C	13.6 5.3
CryoSat-2	8 Apr 2010	Present	717	92°	Ku	13.6
HY-2A	15 Aug 2011	Present	971	99.3°	Ku C	13.58 5.25
SARAL/Altika	25 Feb 2013	Present	800	98.55°	Ka	35.75

in which:

$$\dot{\Omega} = -\frac{3}{2}nJ_2 \left(\frac{R_e}{a}\right)^2 \cos i (1-e^2)^{-2} \ , \tag{2.2}$$

$$\dot{\omega} = -\frac{3}{4}nJ_2 \left(\frac{R_e}{a}\right)^2 (1-5\cos^2 i)(1-e^2)^{-2} \ , \tag{2.3}$$

$$\dot{M} = n - \frac{3}{4}nJ_2 \left(\frac{R_e}{a}\right)^2 (1-3\cos^2 i)(1-e^2)^{-\frac{3}{2}} \ , \tag{2.4}$$

and $T_u = \frac{2\pi}{\dot{\omega}+\dot{M}}$, $T_\Lambda = \frac{2\pi}{\omega_e - \dot{\Omega}}$.

If equations 2.2– 2.4 are substituted in equation 2.1 for a circular orbit, i.e. e=0, we come up with the following equation:

$$\frac{\beta}{\alpha} = \frac{n}{\omega_e} \left\{ 1 - \frac{3}{2}J_2 \left(\frac{R_e}{a}\right)^2 \left(4\cos^2 i - \frac{\beta}{\alpha}\cos i - 1\right) \right\}^{-1} \ . \tag{2.5}$$

This equation describes the relationship between satellite mean motion, n, semi-major axis, a, inclination angle, i, number of revolution, β and repeat cycle, α. In this equation $J_2 = -C_{20}$, ω_e is the angular velocity of the earth and R_e is the earth radius.

2.1.1 Sub-cycle

A sub-cycle is a period of time smaller than the repeat period after which the satellite provides approximately homogeneous global sampling but sparser than that satellite would do during a complete cycle. In the other word one can define the sub-cycle as the time interval between two same neighboring passes, i.e. two ascending or two descending passes. The sub-cycle is an interesting parameter to measure how fast an orbit reduces the large gap at an arbitrary parallel, e.g. equator, when only ascending or descending tracks are considered. Envisat has a 35 days repeat orbit with 16 days sub-cycle. Figure 2.2 shows all ascending ground tracks of Envisat after 16 days at the equator. Sentinel-3 and SWOT have 27 and 21 days repeat orbit with 4 and 10 days sub-cycles respectively. For hydrological purposes an orbit with sub-cycles is preferred because during a short time an altimeter can provide more observations over a given inland water body. For example Envisat every 16 days (sub-cycle) measures Issykul lake (located in Kyrgyzstan) whereas it's repeat cycle is 35 days. Therefore we have more altimetry data over such a lake that is interesting for hydrologists. Another advantage of an orbit with shorter sub-cycle is related to flood management. During the flood seasons we need measurements with more temporal resolution to control flooded area. An altimeter with a shorter sub-cycle orbit can capture flood events. Therefore the short sub-cycle could be an advantage in repeat orbit design for satellite altimetry mission in hydrological applications. Figure 2.1 shows the ground track of Envisat over Issykul lake for one repeat cycle.

Table 2.2: *Repeat orbit of different missions*

Mission	Number of revolution	Repeat cycle (day)	Sub-cycle (day)	Inclination
Envisat	501	35	16	98.60°
CryoSat-2	5344	369	30, 85	92.00°
Sentinel-3	385	27	4	98.65°
SWOT	292	21	10	77.60°

Table 2.3: *Ground track separation at the equator* (km)

Mission	After 10 days	After sub-cycle	After full repeat cycle
Envisat	280	174.0	80.0
CryoSat-2	277	92.2, 32.5	7.5
Sentinel-3	281	703.0	104.0
SWOT	288	288.0	137.0

Figure 2.1: *Envisat satellite ground track during the repeat cycle over Issykul lake*

2.1.2 Coverage pattern

A coverage pattern shows the ascending or descending ground track density along an arbitrary parallel. It is a useful graphical tool to represent relationship between spatial and temporal sampling. If we consider a repeat mode β/α, we can analytically compute the ground track density along an arbitrary parallel. The ground track interval after one day, $2\frac{\pi}{\beta}\alpha$, is called fundamental interval. A fine interval, s_i, is the angular distance between two neighboring ascending nodes after β revolutions, $s_i = 2\pi/\beta$.

Each repeat orbit has a special coverage pattern for example figures 2.2– 2.4 show different equatorial coverage patterns for Envisat, Sentinel-3 and SWOT respectively during the sub-cycle.
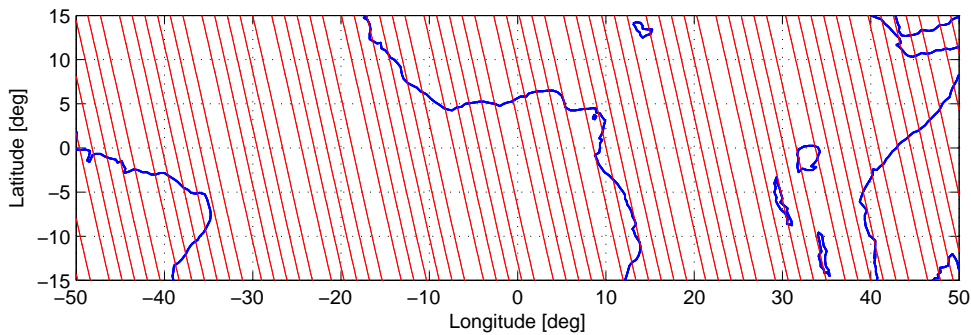
Figure 2.2: *Coverage pattern of Envisat during the sub-cycle time (β=501 and α=35)*
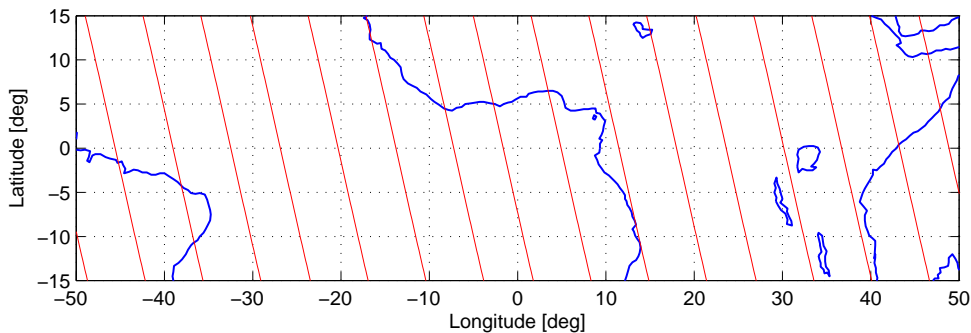
Figure 2.3: *Coverage pattern of Sentinel-3 during the sub-cycle (β=385 and α=27)*
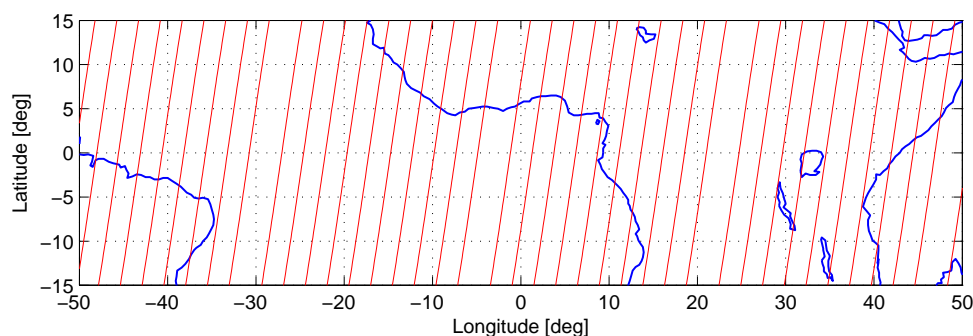
Figure 2.4: *Coverage pattern of SWOT during the sub-cycle (β=292 and α=21)*

2.1.3 Gap evolution

To analyze the spatial and temporal resolution a so-called gap evolution graph is used. This graph shows how fast an orbit samples the large gap(Altés et al., 2010). Figure 2.5 indicates that after 16 days the maximum and minimum gap width are getting closer to each other, i.e. after this time satellite provides a global homogeneous coverage. But for the orbit shown in figure 2.6 the maximum and minimum gap width converge after 35 days, i.e. after its repeat period. So the orbit shown in figure 2.5 is faster than the orbit in figure 2.6 to sample the gap. For a given orbit only being fast (in sampling the gap) is not enough, we must consider its spatial resolution too. For an orbit the higher temporal sampling corresponds to the shorter repeat orbit period and the sparser ground tracks, i.e. satellite only observes the larger inland water bodies. On the other hand the higher spatial resolution needs a longer repeat orbit period that does not satisfy hydrology purposes. Orbits can be classified as drifting orbits and skipping orbits (Altés et al., 2010). In the first type, each track occurs next to previous one. In this type of orbits sampling fundamental interval will be completed progressively. Figure 2.6 indicates a drifting orbit. From this figure we can see that the maximum and minimum gap curves are getting closer to each other slowly. In the second type of orbit, the fundamental interval is sampled in a more random way and filling the large gap in the fundamental interval is faster than that would do by drifting orbits.

2.2 Altimeter measurement principle

A radar altimeter mounted on the satellite sends pulses with a known power and frequency to the earth surface. One part of these signals reflects at the surface and is received by the altimeter. The radar system measures the time τ for the pulse to travel round trip between the satellite and the earth surface. The round trip travel time is:

$$\tau = 2\frac{R}{c} \quad , \tag{2.6}$$
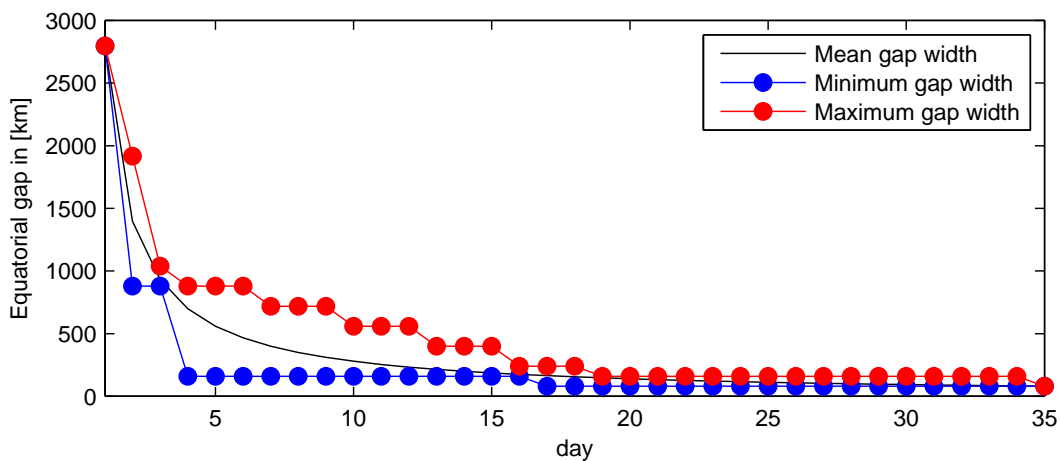
Figure 2.5: *Gap evolution graph for a skipping orbit, β=501 and α=35*
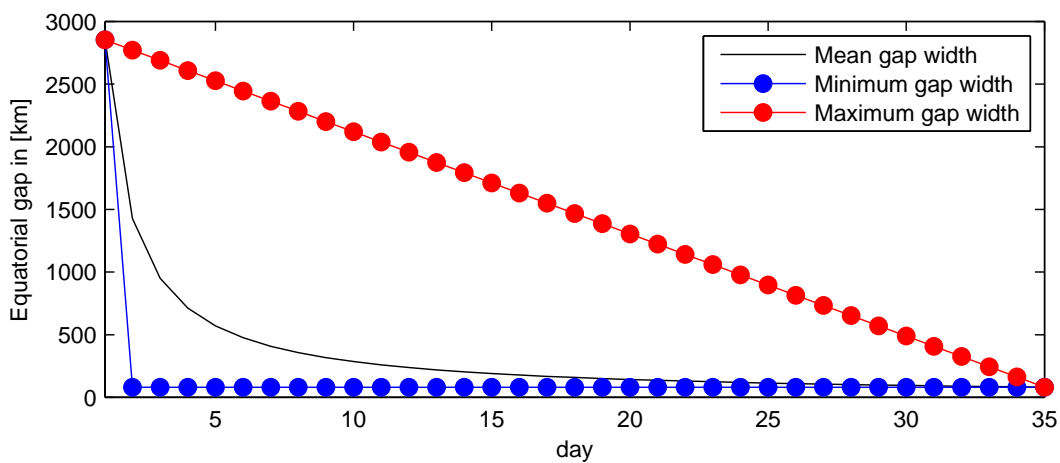
Figure 2.6: *Gap evolution graph for a drifting orbit, β=491 and α=35*
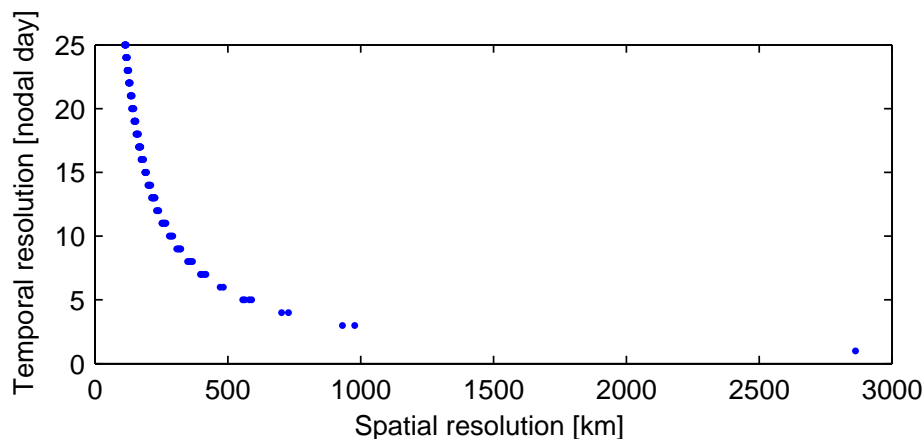
Figure 2.7: *Spatial and temporal resolution for orbits with repeat cycle less than 25 days*

in which c is speed of light. Then the range from the satellite to the surface is determined from:

$$R = \frac{1}{2}c\tau \ , \tag{2.7}$$

R is a row range that needs to be corrected:

$$R = c\frac{\tau}{2} - \sum_i \Delta R_i \ , \tag{2.8}$$

in which ΔR_i are the range corrections including (Fu and Cazenave, 2001):

- Dry troposphere
- Wet troposphere
- Ionosphere
- Solid earth tide
- Pole tide .

2.2.1 Radar equation

If an isotropic antenna (an antenna which emits radiation uniformly in all directions) transmits signals with power P_t, the amount of received energy at range r is $P_t \frac{1}{4\pi r^2}$ (Rosmorduc et al., 2011). The signals propagate uniformly in all directions at the transmitted power. Antenna gain pattern, G provides more radiation in the nadir direction. So the directional power density increases as $P_t \frac{1}{4\pi r^2} G$. The size and scattering properties of a target inside the antenna footprint,
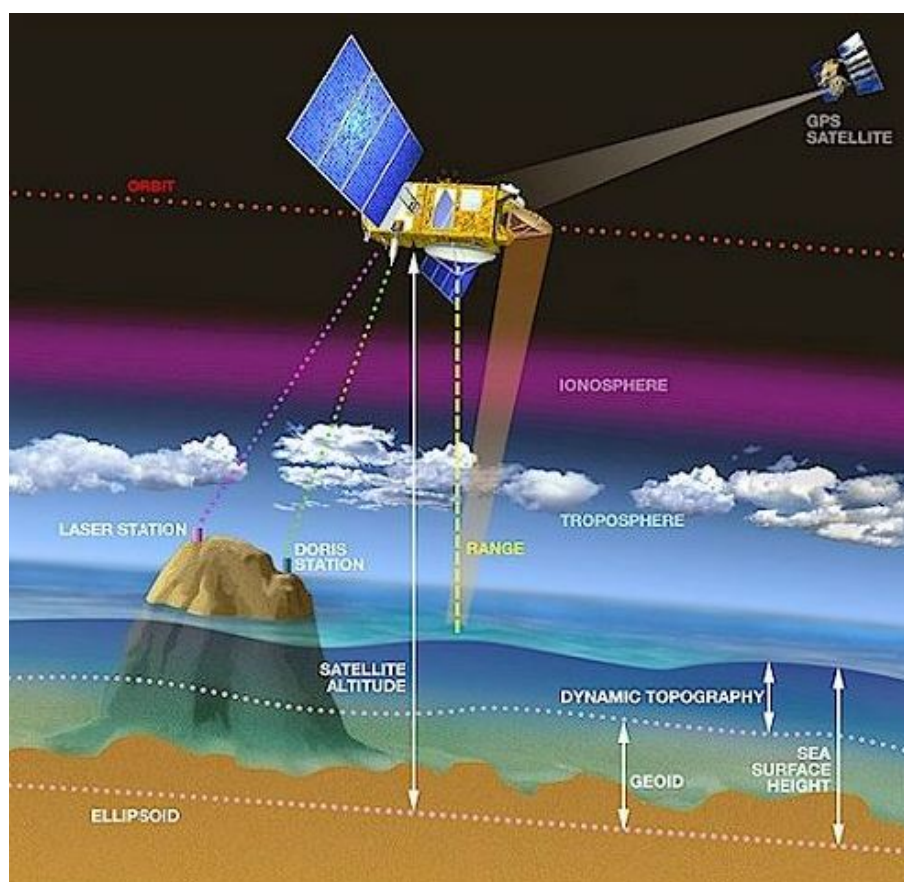
Figure 2.8: *Basic measurement principle of the satellite radar altimeter to measure the sea surface height (http://www.altimetry.info)*

σ, known as radar cross-section affects the radar signal. So the power intercepted by the target is $P_t \frac{1}{4\pi r^2} G \sigma$. According to Kirchhoff's law the ratio of emissivity and absorptivity is constant (Kleusberg and Wild-Pfeiffer, 2008). Therefore the reflected power density back at range r is $P_t \frac{1}{4\pi r^2} G \sigma \frac{1}{4\pi r^2}$. This is the power intercepted by a radar antenna whose effective area is A_e, so the received power P_r is given by :

$$P_r = \frac{P_t G}{4\pi r^2} \sigma \frac{1}{4\pi r^2} A_e \quad . \tag{2.9}$$

$A_e = A\, K_a$ in which K_a is efficiency. A_e is related to antenna gain by $G = \frac{4\pi A}{\lambda^2}$ (λ is the wavelength and A is the geometrical antenna area), So the radar equation can be written in the more useful form:

$$P_r = \frac{P_t G^2 \lambda^2 \sigma}{(4\pi)^3 r^4} \quad . \tag{2.10}$$

2.2.2 Backscatter coefficient

One of the fundamental measurements of satellite altimetry is the ratio of the received signal power at the antenna and the transmitted signal power from the antenna. After the signals are transmitted from the radar, they are attenuated by atmosphere then they arrive at the water surface. Some of the power is scattered back and some of them is absorbed by water. The reflected part during the pass to the radar is attenuated again by atmosphere and the rest received by radar antenna. The backscatter coefficient, called normalized radar cross section (http://www.altimetry.info), is quite difficult to estimate and is normally determined by measurement. We suppose that the backscatter coefficient σ is spatially homogeneous over the area inside the antenna footprint. Therefore from the radar equation one can compute the backscatter coefficient:

$$\sigma = \frac{P_r (4\pi)^3 r^4}{P_t G^2 \lambda^2} \quad . \tag{2.11}$$

2.2.3 Area illumination and waveform construction

A pulse-limited altimeter employs a nadir-pointing radar to transmit a short pulse with a duration of few nanoseconds from the antenna. In the case of Envisat, RA2 radar sends pulses with two frequencies 13.575 GHz for the Ku-band and 3.200 GHz for the S-band (https://earth.esa.int/handbooks/Envisat). The shape of the reflected signal, called waveform, indicates the time evolution of the reflected power as the radar pulse hits the water surface. The waveform is the basic measurement to observe geophysical parameters of the earth surface (Anzenhofer et al., 1999). It provides information about the properties and nature of the reflecting surface such as significant wave height and backscatter coefficient. Figure 2.10 represents the story behind the waveform construction. The radar antenna transmits an electromagnetic pulse toward the surface beneath the satellite that propagates in the spherical wavefront shape. The wavefront hits the surface at $t=t_0$, it illuminates one point and a reflected power starts to return to the altimeter. As time goes on the pulse progresses and the wavefront reaches the other points away from nadir point and forms a disc. Within the

Table 2.4: Summary of instrument characteristics of altimeter missions (http://www.aviso.altimetry.fr)

Altimeter	Band	Antenna beamwidth	PRF[1] (Hz)	Number of waveform gates	Nominal tracking point	Gate width (ns)
Geosat	Ku	2.00°	1020	60	30.5	3.125
ERS-1	Ku	1.30°	1020	64	32.5	3.030
Topex	Ku	1.10°	4500	128	32.5	3.125
	C	2.70°	1200	128	32.5	3.125
Poseidon	Ku	1.10°	1700	60	29.5	3.125
ERS-2	Ku	1.30°	1020	64	32.5	3.030
GFO	Ku	1.60°	1020	128	32.5	3.125
Jason-1	Ku	1.28°	1800	104	31.0	3.125
	C	3.40°	300	104	31.0	3.125
Envisat	Ku	1.29°	1800	128	46.5	3.125
	S	5.50°	450	64	25.5	6.250
Jason-2	Ku	1.26°	1800	104	31.0	3.125
	C	3.38°	300	104	31.0	3.125
CryoSat-2, LRM	Ku	1.08°, 1.20°	1970	128	63.0	3.125
CryoSat-2, SAR	Ku	1.08°,1.20°	18181	128	63.0	1.562
CryoSat-2, SARIn	Ku	1.08°,1.20°	18181	512	255.0	1.562
HY-2A	Ku	41.00°,49.00°	2000	128	32.5	3.125
	C	41.00°,49.00°	2000	128	32.5	6.250
SARAL/Altika	Ka	1.29°	1800	128	46.5	3.125

1: Pulse Repetition Frequency
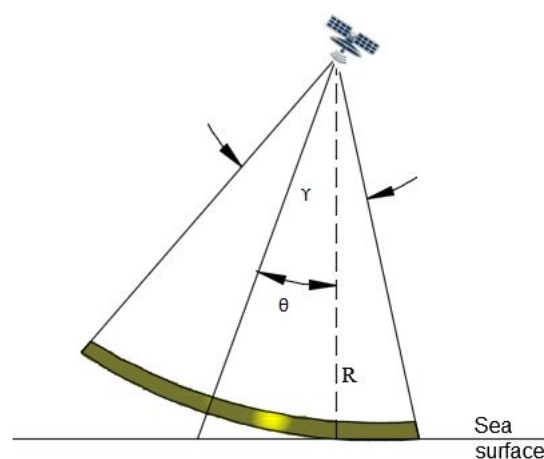
Figure 2.9: Geometry of pulse-limited altimeter (Fu and Cazenave, 2001)

disc, backscatter power reaches the radar and builds up rapidly rising part of the waveform (leading edge). The maximum return power corresponds to the occasion of maximum area of disc, $t=t_1$ (Deng, 2003). After t_1 this disc transits to annular ring and the power begins to decay. The reflected signal back to the radar from the ring, generates the next part of waveform with long decay (trailing edge). The first part of the waveform is thermal noise in the radar. For time tracking purposes returned signals are averaged on-board usually every 50 ms (https://earth.esa.int/handbooks/Envisat) and recorded within the tracking window (128 gates for the Ku band and S band with 64 gates for Envisat). In figure 2.11 one can find the components of the waveform with ideal shape over the open ocean. It mainly includes three parts:

- The thermal noise adds a constant power level to the returned waveform.

- The leading edge contains the returned power from the scattering surface within the footprint of the radar which gives us information about range and significant wave height.

- The trailing edge contains the returned power from the scattering surface outside the footprint of the radar.

The averaged returned waveform is a time series of mean returned powers referred to as the Brown model explained by convolution of three components (Brown, 1977) (Hayne et al., 1994):

$$W(t) = P_{\text{fs}}(t) * Q_{\text{s}}(t) * S_{\text{r}}(t) \ , \tag{2.12}$$

where P_{fs} is the average flat surface response, Q_{s} is the probability distribution density function of specular points in the radar footprint and S_{r} is the radar system point target response.

2.2.4 Water level from altimetry measurements

From the altimetry measurement principle one can determine water level of an inland water body. Based on the altimetry principle shown in figure 2.8 the water level is the difference between the satellite orbit height,H, and the measured range, R, so we can write:

$$h = H - R \ , \tag{2.13}$$

in which H is the satellite altitude above the ellipsoid, R corrected range and h is the water height above the ellipsoid. It is worthy to mention that altimeters provide ellipsoidal height, h. Therefore h differs from physical height. From equation 2.13 one can say that with a precise orbit determination and a precise range measurement the error of h is decreased. The orbit determination is a wide area for study and research, we don't want to discuss it here. Therefore we only focus on the range measurements and dealing with algorithms and techniques in data processing that provide the smaller error for R to determine the more precise water level.
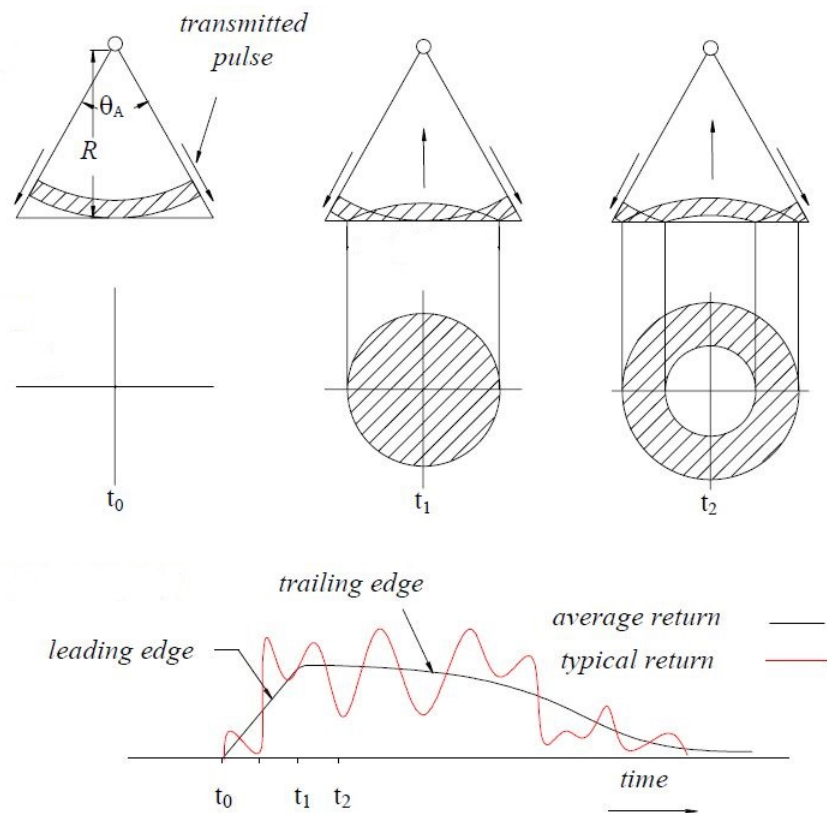
Figure 2.10: *Schematic geometrical description of the interaction of a pulse and scattering surface and build up of a returned waveform over the duration of a pulse (Deng, 2003)*
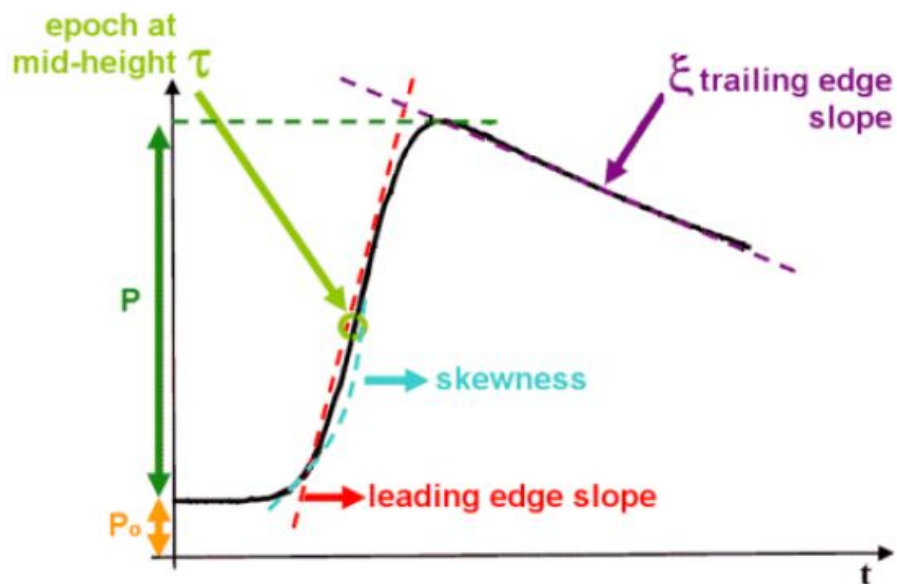
Figure 2.11: *The basic schematic outline of a waveform over the open ocean, ideal shape for the waveform (http://www.altimetry.info)*

Chapter 3

Data and area of study

3.1 Data

In this study we used Envisat RA2 GDR (Geophysical Data Record) and SGDR (Sensor Geophysical Data Record) data. These data cover the complete time span of the Envisat mission from May 2002 to April 2012 that corresponds to cycles 06–113. The European Space Agency (ESA) launched the Environmental Satellite (Envisat) in March first 2002 to continue the ERS-1 and ERS-2 missions. Envisat carried 10 instruments including RA2 (Advanced Radar Altimetry) and flew in an orbit with $98.6°$ inclination and 35 day repeat period that covers all of the area between $-81.4°$ to $+81.4°$ latitude. RA2 was a high precision nadir radar altimeter that operated at two frequencies $13.575\,$GHz and $3.200\,$GHz, corresponding to $2.3\,$cm and $3.4\,$cm wavelength in Ku-band and S-band respectively (Santos et al., 2010).

RA2 GDR data, distributed by ESA, fulfills needs of the most scientific researchers. This data includes time of range measurements, ranges, satellite positions, geophysical corrections, media corrections and other information. For the range measurements four different tracking and retracking algorithms, i.e. ocean, sea ice, ice-1 and ice-2 are operationally applied to RA2 raw data to provide accurate height estimates (Frappart et al., 2006). Each retracker has been developed to a specific surface response.

RA2 SGDR includes RA2 GDR, clusters of $18\,$Hz waveform data and additional information. We are interested only in GDR and Ku-band waveform data. For more information about RA-2 files please look at the http://earth.esa.int/pub/ESA_doc/Envisat/RA2/.

For validation of water level obtained from satellite measurements we used daily in-situ gauge time series of one station (SADRA private company, http://www.sadra.ir/). This data covers the span time from September 1965 to August 2004 that has the overlap of about 2 years with satellite measurements. In-situ gauge height is referenced to geoid, EGM96. This data has sufficient temporal resolution to assess the water level precision from satellite altimetry data.

3.2 Area of study

The area of study in this research is Urmia lake. Urmia in Assyrian means city of water. In the 9th century BCE two names were mentioned for Urmia lake that came from Assyrian records: *Parsuwash* and *Matai*. Urmia lake was titled as Kabodan (extracted from persian word " azure", means blue) and Chichast (glittering mineral particles suspended in the lake water

and found along its shores). Before the Iran revolution its name was Razaiyeh referring to Reza Shah Pahlavi, the king of Iran (1941–1979). Since the 1970s it has been renamed as Urmia, *(http://en.wikipedia.org/wiki/Lake Urmia, Last visit, Nov 2014)*.

Lake Urmia, located in the Northwest of Iran, near Iran's border with Turkey, is a hypersaline and endorheic lake which means that it retains water and allows no outflow to other external water bodies. Located between the Iranian provinces of East and West Azerbaijan, it is the largest lake in the Middle East and the third largest salty water lake on earth. It had a dimension of 140 km length, 55 km width and 16 m depth also its surface area was about 6100 km^2 in 1995 but it has been declining and was estimated about 2366 km^2 in August 2011 (Pengra2012). The recent study (Tourian et al., 2015) shows the lake has lost 70% of its surface area during the last 14 years with an average rate of 220 km^2 yr^{-1}.

The mean position (longitude and latitude) of Urmia lake is $\lambda = 45.42°$ and $\varphi = 37.72°$. Lake Urmia is protected as a national park.

Figure 3.1: *Urmia lake and position of different dams in its basin (Pengra et al., 2012)*

Chemical elements in the water of Urmia lake mainly including cations such as Na$^+$, K$^+$, Ca$^+$, Li$^+$ and Mg^{2+} and anions such as Cl$^-$, SO$_4^{2-}$ and HCO$_3^-$. The Na$^+$ and Cl$^-$ concentration is roughly 4 times the concentration of natural seawater. Sodium ions are at slightly higher
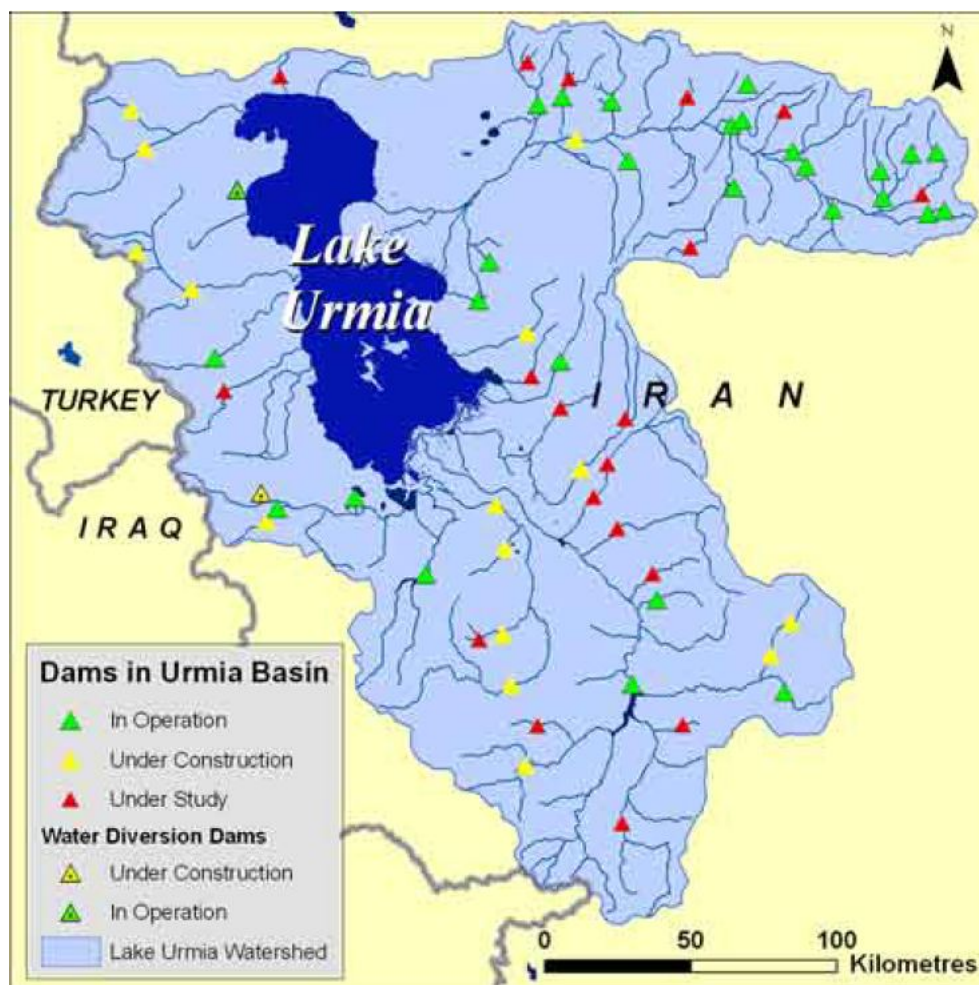
concentration in the south compared to the north of the lake, which can be results from the shallower depth in the south and the higher evaporation rate (Asem et al., 2012).

The lake has been divided into north and south parts by a causeway with a length of 1500 m that provides little exchange of water between the two parts. Due to drought and increased demands for irrigation water in the lake's basin, the salinity of the lake has risen to more than $300 \, \text{g} \, \text{l}^{-1}$ during recent years and a large area of the lake bed has been fallen dry (Asem et al., 2012).

Urmia lake is home to 212 species of birds, 41 reptiles, 7 amphibians, and 27 species of mammals including the Iranian yellow deer. The lake is marked by more than a hundred small rocky islands, which are stopover points for the various wild migration birds such as flamingos, pelicans and spoonbills. It has been registered as an international protected area by UNESCO Biosphere Reserve (Rezvantalab and Amrollahi, 2011).

The last decay drought has significantly reduced the inflow water in to the lake that caused increasing the salinity of the lake's water and lowering the lake viability. The salinity has increased specially in the southern half of the lake. Because of high salinity, there is no fish life. Nevertheless Urmia lake is considered as a significant natural habitat of Artemia which serve as a food source for the migratory birds such as flamingos (*http://en.wikipedia.org/wiki/Lake Urmia, Last visit Nov. 2014*).

This lake is a major barrier between the two provinces West Azerbaijan and East Azerbaijan. A project to construct a highway across the lake was initiated in the 1970s. But it was abandoned after the Iranian revolution in 1979, having finished a 15 km causeway with an un-bridged gap. The project was revived in the early 2000s, and was completed in November 2008 with the opening of a 1.5 km bridge across the remaining gap (*http://en.wikipedia.org /wiki/Lake Urmia, Last visit Nov. 2014*). Experts have warned that the construction of the causeway and bridge, together with a series of ecological factors, will eventually lead to the drying up of the lake, turning it into a salt marsh which will directly affect the climate of the region. Lake Urmia has been shrinking for a long time. Tourian et al. (2015) recently showed an alarming rate of about $1.03 \, \text{km}^3 \text{yr}^{-1}$ in terms of water loss for this lake.

Responsible organizations did not pay attention to the problem at the beginning but after some demonstrations by local people against this critical situation, the government promised to find a solution to revive the lake. They believe there are two possibilities. One solution could be to increase inflow water from inside the watershed by making some limitation for surface and ground water consumption for irrigation. The other is transferring water outside the watershed, from Caspian sea and Aras or Zab rivers (Pengra et al., 2012). But unfortunately each solution has special own problem. A restricted use of water for irrigation is a serious menace for agricultural products which are the most important economical factors in this area of Iran. Also transferring water from other water bodies located in border zone and long distance from Urmia lake is very expensive. Besides an agreement with the other countries is necessary that would not be easy to achieve.

Urmia lake plays a very important role in the ecosystem of northwest of Iran. Keeping this role requires monitoring water level and studying runoff and catchment of the lake. As Urmia lake is endorheic water body there is no considerable water volume outflow other than that by evaporation. During the last decade Iran Water and Power Resource Development Co. (IW-PCo), a major responsible organization for dam and hydroelectric power projects, has started to build a lot of dams on the inflow rivers to the lake. Unfortunately most of these projects are

running without comprehensive pre-analysis and without considering practical influences on the local ecosystem. Therefore dam construction has significant contribution to reduce water budget of Urmia lake. On the other hand less precipitation during last decade leads to increase reduction water level of the lake. Previous studies (Pengra et al., 2012) show that 65% of declining water comes from changing of inflow to the lake due to climate changes and diversity using of upstream water. Decreasing precipitation contributes by 10% and dam construction exacerbates reduction of water budget of the lake by 25% (Pengra et al., 2012).

If the desiccation continues at the current rate (Tourian et al., 2015) in the near future the lake will completely be dry. That could be a big threat for destruction of civilian and wild life in the large area of Iran. Because with a small wind salty-sandy powder of the lake bed will be spread over surrounding area.

Fortunately Envisat satellite altimetry covered Urmia lake by two tracks numbered 371 for the ascending pass and 178 for the descending pass. This coverage is shown in figure 3.2 for one repeat cycle of the satellite revolution.

Figure 3.2: *Envisat satellite ground tracks*

Chapter 4

Water level from on-board tracker and retrackers

GDR data were processed using on-board tracker and retrackers to define water level time series of Urmia lake. We processed these data according to the algorithm described below. The ocean tracker and sea ice, ice-1 and ice-2 retracker algorithms were used on-board of the altimeter RA2 for the range measurements (http://earth.esa.int/pub/ESA_doc/Envisat/RA2/). Since none of these tracker and retracker was dedicated to process altimetry data for inland water bodies, we used all of them to define water level of the lake according to our methodology. We compared the water level obtained from these tracker and retrackers with in-situ gauge data to find the most robust water level estimator. Water level is derived from the satellite orbit height, range measurements and corrections to the range.

4.1 Methodology

To define water level time series derived from GDR data we did the following steps:

- Selecting RA2 GDR data over Urmia lake

- Separating ascending and descending track measurements

- Defining a short water level of the lake from both ascending and descending tracks for each satellite pass over the lake, called instantaneous water level time series, using:

  - ALL

  - MEDIAN

  - MEAN

  values of water level in each pass using ocean tracker and ice-1, ice-2 and sea-ice retrackers.

- Fitting a linear trend to the instantaneous water level time series (from a given pass) to detect and delete outliers

- Merging all single pass water level time series to create a long time series from all passes separately for ascending and descending tracks

- Fitting a model including linear and quadratic as well as seasonal trigonometric terms to delete outliers from the long time series

- Comparing the time series from ascending and descending tracks to check if there is any systematic error

- Combining ascending and descending track time series to define a united water level time series for the lake

- Comparing combined time series with the in-situ gauge data to find the most robust water level estimator

To select data which covers Urmia lake, a complete cycle (cycle 92) of Envisat data was considered. Based on the longitude and latitude of Urmia lake coastline only those satellite tracks were selected that pass over the lake, tracks 178 and 371. Figure 4.1 (a) indicates all sub-satellite points over Urmia lake from cycle 6 to cycle 113 also it includes the position of an in-situ gauge station. We found out the location of MEDIAN values of water level in each satellite overpass, shown in figure 4.1 (b). Median locations distribute along the tracks but mostly located in the area between $37.6°$ and $37.8°$ latitude.

(a)   *(b)*

Figure 4.1: *Envisat sub-satellite points over Urmia lake from cycle 6 to cycle 113 (a), Location of MEDIAN water level values for each satellite pass (b)*

4.2 Water level time series of the lake from satellite measurements

Fitting the model and outlier rejection

According to our methodology we defined water level time series for each satellite pass using the ocean tracker, ice-1, ice-2 and sea-ice retrackers. A linear trend $h(t_i) = a + bt_i$ was considered to fit to the single pass to eliminate outliers at the confidence level of 95%. Each overpass takes about 18 s and 10 s for ascending and descending tracks respectively. If we consider only
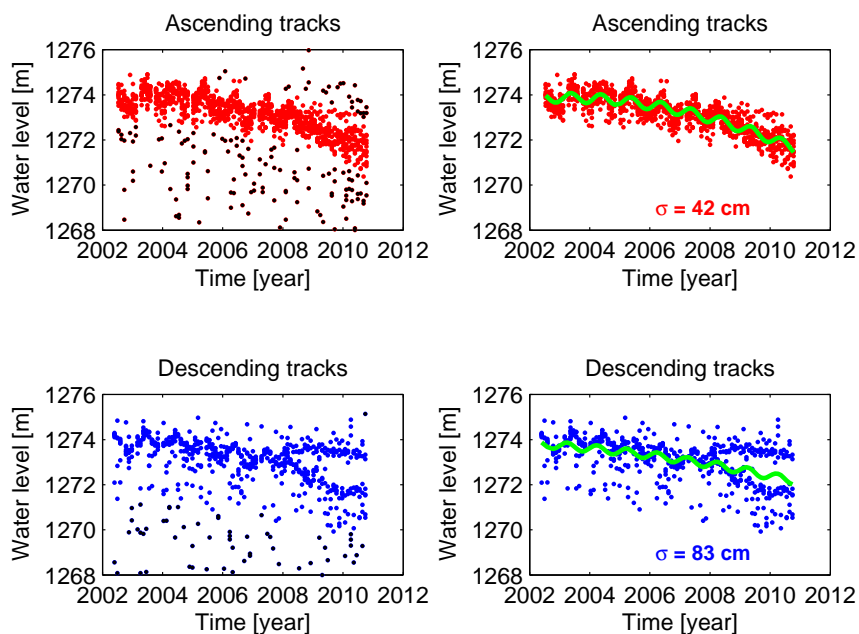
Figure 4.2: *Water level time series based on retracker ice-1 from ALL values of all satellite passes*
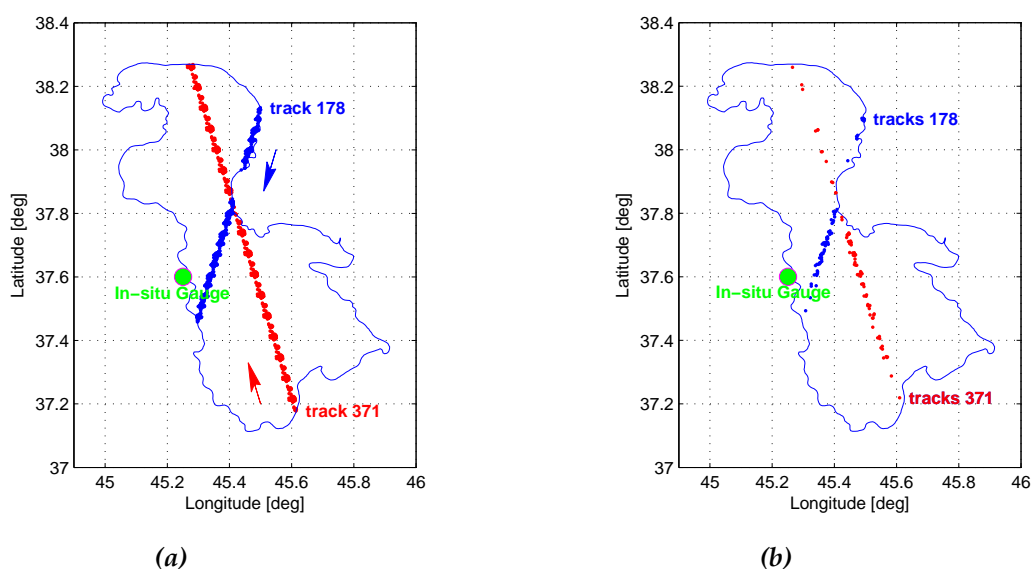

(a)   *(b)*
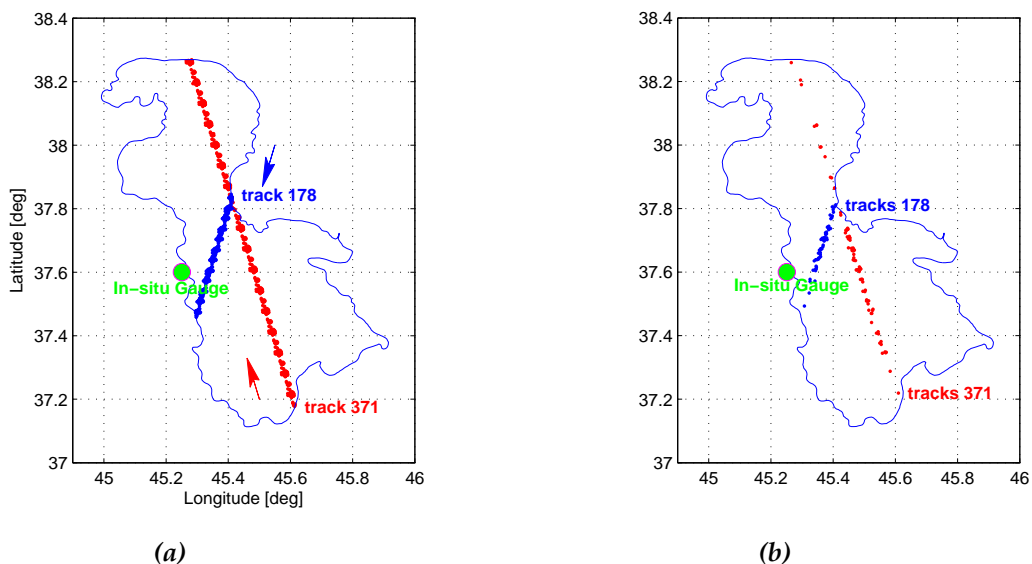
Figure 4.3: *Envisat sub-satellite points over Urmia lake from cycle 6 to cycle 113 (a), Location of MEDIAN water level values for each satellite pass (b)- after removing upper part of the descending tracks*

the mean water level, there is no unexpected water level variations during the short time for a given single pass for water level profiles. Therefore a linear trend would be sufficient to detect and delete outliers. These so called instantaneous water level profiles are shown in figure 4.4. For visual purpose water level of each satellite pass, we shifted the water profiles with respect to each other and plotted them in figure 4.5 at an arbitrary height. Relative height in this step would be enough to see water level changes during each one of these single pass profiles.

From figure 4.1 (a) we see that track 178 is very close to the shoreline. In the shoreline area satellite altimetry waveforms are usually contaminated with signals reflected back from non-water surface. Therefore in these areas we have erroneous ranges. Figure 4.2 shows that after 2008 water level from the descending tracks 178 diverged because of shallow water and land contamination of altimetry measurements above 37.85° latitude. To avoid such an event in figure 4.2 one way is to exclude the upper part of the descending track measurements from data analysis. Another solution is to keep all measurements and to do waveform retracking. We followed the first way in processing GDR data, i.e. removing the upper part of data. As you can see from figure 4.7 (bottom left) data removal works well and it produces a proper water level time series. We discussed about the second solution in chapters 5 and 6.
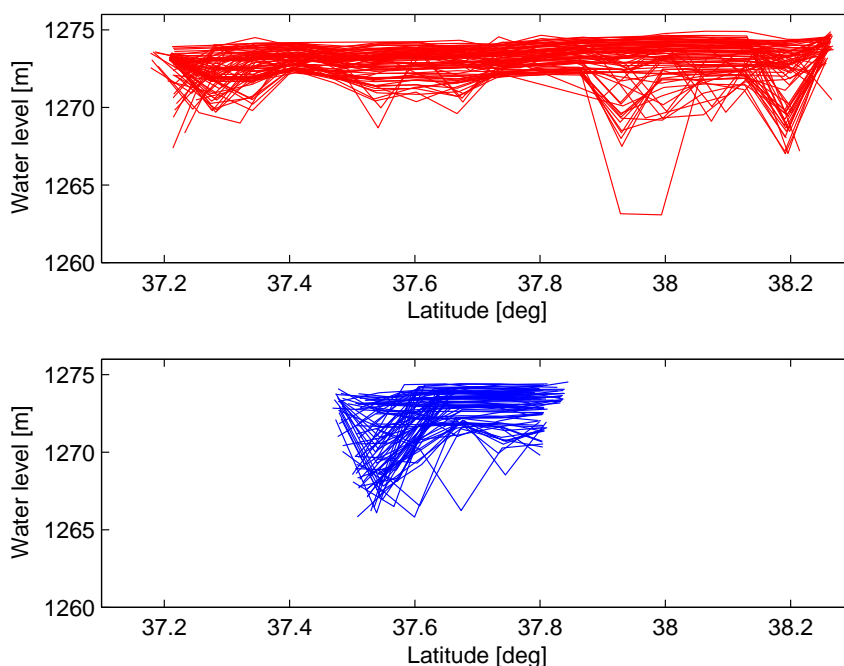
Figure 4.4: *Instantaneous water level profile based on ice-1 retracker from all satellite ascending passes (upper panel) and descending passes (lower panel)*

After removing the near-shoreline data from the descending tracks, we define new short water level time series. Each has a standard deviation, shown in figure 4.6. The mean standard deviation of water level of all passes before outlier rejection are 94 cm and 108 cm but after outlier rejection they are 80 cm and 95 cm for ascending and descending tracks respectively. After preliminary outlier elimination, water level time series are defined for ascending and descending tracks separately from ALL, MEDIAN and MEAN values of water level for each satellite overpass based on the tracker and different retrackers. Figures 4.7– 4.9 show water level time
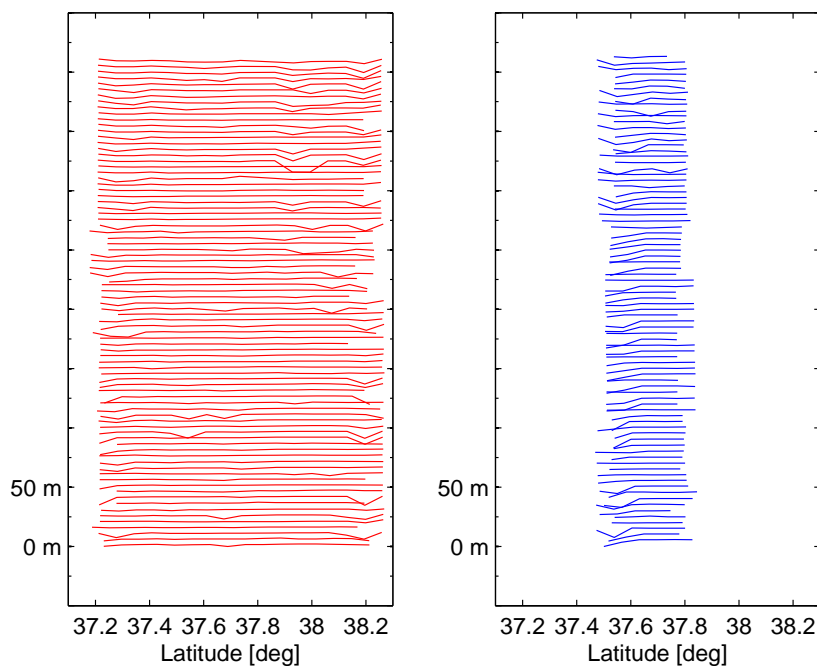
Figure 4.5: *Shifted water level profiles for ascending (left) and descending (right), ice-1 retracker*

series for the ascending and descending tracks using ice-1 retracker from ALL, MEDIAN and MEAN values respectively.

For accurate and valid water level, three kinds of time series (obtained from ALL, MEDIAN and MEAN values) were considered to detect and eliminate probable outliers. To find outliers we consider a model (trend) which can capture permanent and periodic (seasonal) variations of water level of the lake. The model also determines the acceleration of water level variations. This model (equation 4.1) including linear and quadratic as well as trigonometric terms according to linear least squares parametric adjustment method (LLSPA) was estimated and fitted to the time series:

$$h(t_i) = a + bt_i + ct_i^2 + d \sin\left(\frac{2\pi}{T}t_i\right) + e \cos\left(\frac{2\pi}{T}t_i\right) \quad . \tag{4.1}$$

In which a, b, c, d and e are unknown parameters that must be estimated. T is the annual period and h is the observed water height. This trend was removed from the time series. For the residual a statistical test at 95% confidence level was performed in an iterative way. Tables 4.1– 4.3 show the standard deviation of the residuals of water level before and after outlier removal. They also include the number of observations and the number of outliers. Black dots in figures 4.7– 4.9 are the identified outliers. We are interested in two statistic parameters as quality measures for analyzing the performance of the tracker and retrackers:
1- σ: the standard deviation of residuals of water level (time series - trend), hereafter we simply call it the standard deviation,
2- RMS: first the RMS measures the difference between ascending and descending track water level time series (ascending track time series - descending track time series) then it measures
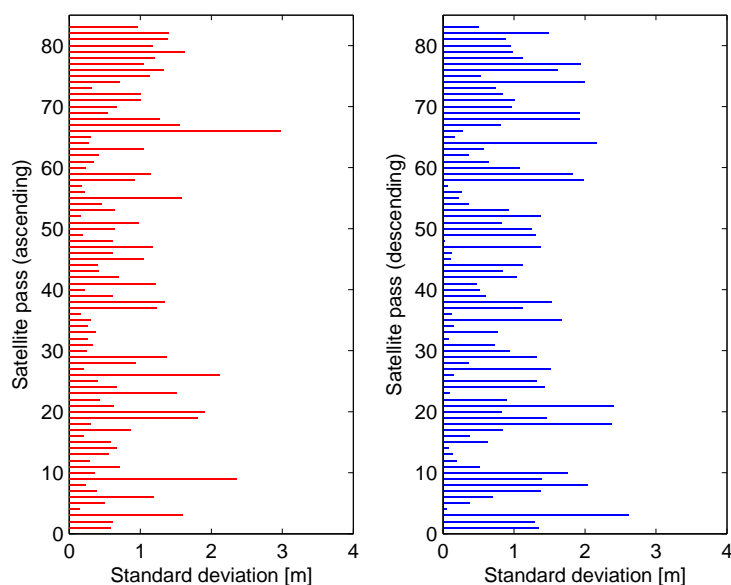
***Figure 4.6:** Standard deviation of each instantaneous water level time series after outlier rejection for ascending (left) and descending (right), ice-1 retracker*

the difference between combined water level time series from ascending/descending tracks and the in-situ gauge time series (combined time series - in-situ gauge time series).

The standard deviation σ is only showing internal validation but RMS is showing both internal and external validations. After removing outliers, the observations from ascending and descending tracks were combined to build a united water level time series. The model described in equation 4.1 was fitted to this time series to find and reject all possible outliers. Table 4.5 includes the standard deviations after this combination. Also figures 4.10– 4.12 (the lower panels) illustrate this combination for ALL, MEDIAN and MEAN values based on retracker ice-1.

Result of ALL values
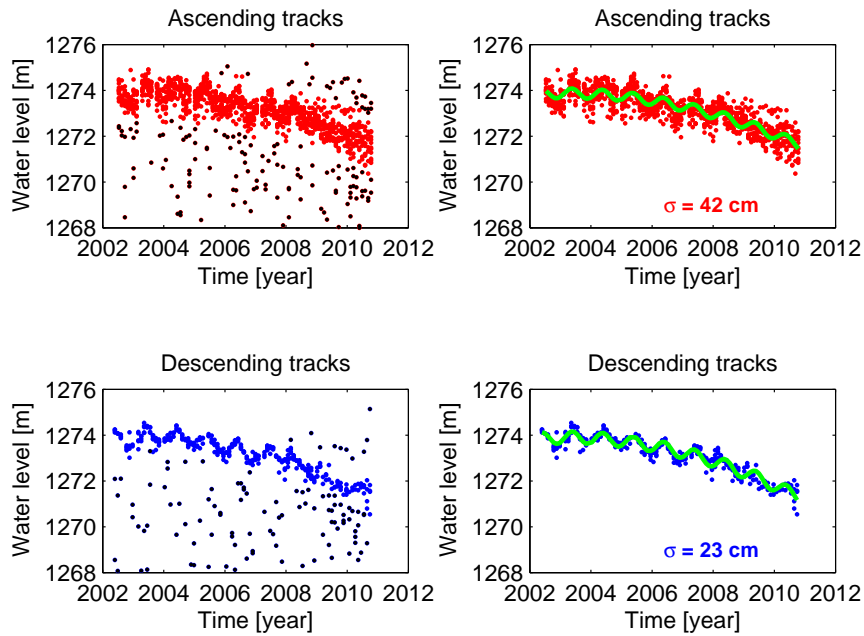
Figure 4.7: *Water level time series from the ALL values of ascending and descending tracks based on ice-1 retracker*

Table 4.1: *Standard deviation* (cm) *for ALL values*

retracker	ascending tracks				descending tracks			
	before	after	no. out[1]	no.obs[2]	before	after	no. out	no.obs
ice-1	120	**42**	161	1309	192	**23**	103	455
ice-2	92	70	146	1309	161	37	103	455
sea-ice	242	65	202	1309	342	208	32	455
ocean	352	81	175	1309	282	147	31	455

1: number of outliers   2: number of observations

Result of MEDIAN values
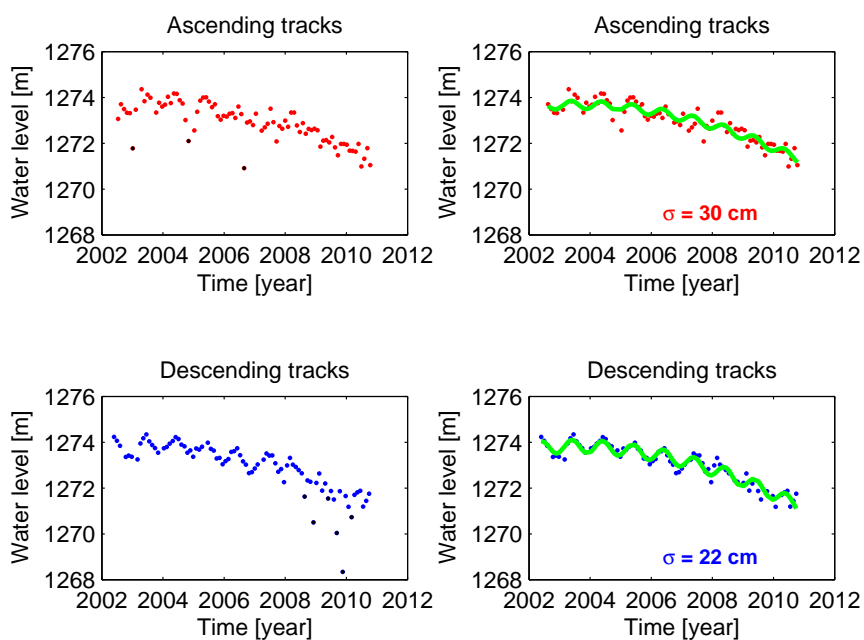
Figure 4.8: *Water level time series from the MEDIAN values of ascending and descending tracks based on ice-1 retracker*

Table 4.2: *Standard deviation* (cm) *for MEDIAN values*

retracker	ascending tracks			descending tracks			no. obs
	before	after	no. out	before	after	no. out	
ice-1	49	**30**	3	84	**22**	6	83
ice-2	172	85	3	44	19	5	83
sea-ice	120	72	6	275	105	8	83
ocean	124	81	2	85	36	7	83

Result of MEAN values
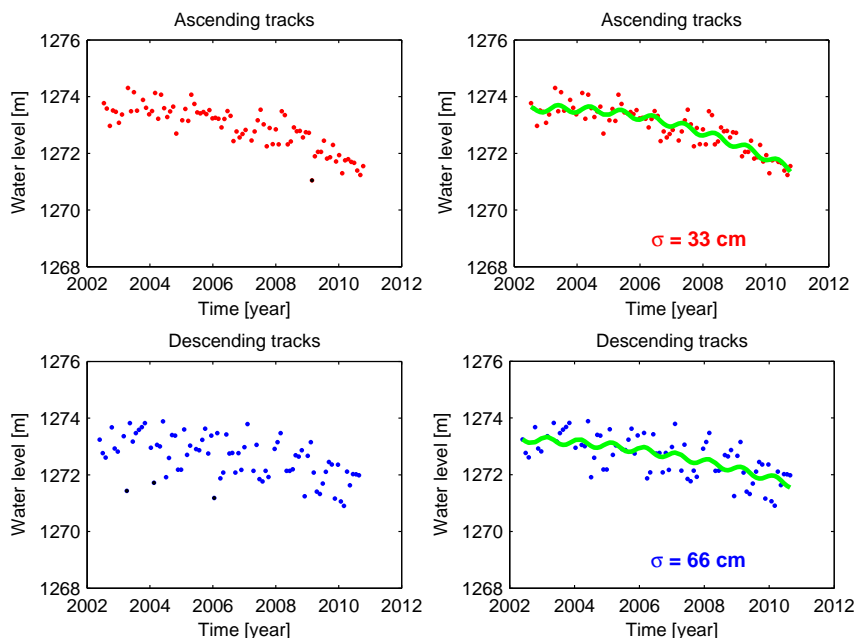
Figure 4.9: *Water level time series from the MEAN values of ascending and descending tracks based on ice-1 retracker*

Table 4.3: *Standard deviation* (cm) *for MEAN values*

retracker	ascending tracks			descending tracks			no. obs
	before	after	no. out	before	after	no. out	
ice-1	36	33	1	86	55	6	83
ice-2	32	**30**	52	63	**21**	48	83
sea-ice	76	76	0	130	86	12	83
ocean	67	45	36	117	41	45	83

4.3 Water level from in-situ gauge measurements

Measurements from an in-situ gauge station located on figure 4.1 was used. The water level time series of this station spans from September 1965 to August 2004, shown in figure 4.13. This figure also includes water level time series obtained from satellite measurements. For comparison we used only one part of the time series which has overlap with Envisat data, i.e. from May 2002 to August 2004. Figure 4.14 indicates water level time series from ALL, MEDIAN and MEAN values based on ice-1 retracker respectively corresponding to the in-situ gauge readings.

4.4 Validation

4.4.1 Internal validation

Defining water level time series separately from the ascending and descending tracks provides an opportunity to asses the quality of altimetry data. Figures 4.11 and 4.12 (the upper panels) indicate that there is consistency between water level from the ascending and descending tracks specially for MEDIAN values based on re-tracker ice-1. Table 4.4 shows the difference between the average water level from ascending and descending tracks. The maximum difference (for seaice retracker) is less than 0.5 m. From this table and figures 4.10– 4.12 one can see that there is no bias and systematic error between water level from the ascending and descending tracks.

For internal validation the RMS of water level between the ascending and descending tracks was computed for ALL, MEDIAN and MEAN values based on different retrackers. To compute the RMS, water level time series defined from the ascending tracks was interpolated linearly to find corresponding water level at the epochs of the descending tracks. The solid-dot black curves in figures 4.10– 4.12 show the interpolated water level values of the ascending tracks.

Table 4.4: Difference between the average water level (cm) *from ascending and descending tracks*

retracker	all	median	mean
ice-1	1	17	28
ice-2	3	34	35
seaice	43	7	20
ocean	22	14	28

Table 4.5: Standard deviation (cm) *after the combination of ascending and descending tracks*

retracker	all	median	mean
ice-1	39	**27**	48
ice-2	63	75	35
seaice	134	84	82
ocean	112	82	49

4.4.2 External validation

Water level from the in-situ gauge is an independent data set to control the quality of the water level obtained from altimetry data. For the external validation the in-situ gauge time series was interpolated linearly to find water level corresponding with the water level defined from the combined satellite ascending and descending tracks. Then the RMS values of water level between in-situ gauge and satellite data were computed for ALL, MEDIAN and MEAN values. The numerical result is in table 4.6. Figure 4.14 shows the water level time series derived from
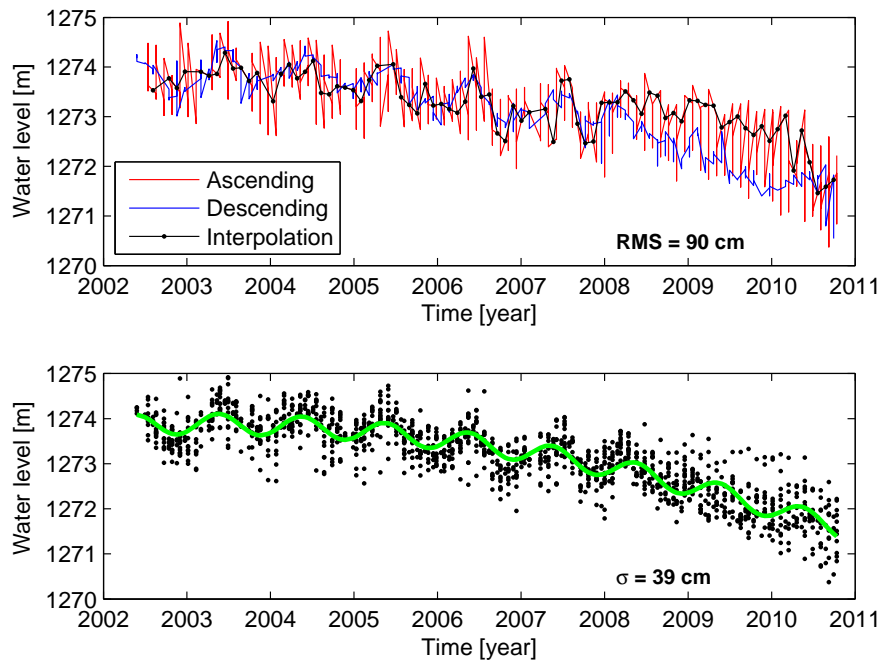
Figure 4.10: *Comparing water level from the ascending and descending tracks (upper panel), combined water level time series (lower panel) - from the ALL values based on ice-1 retracker*
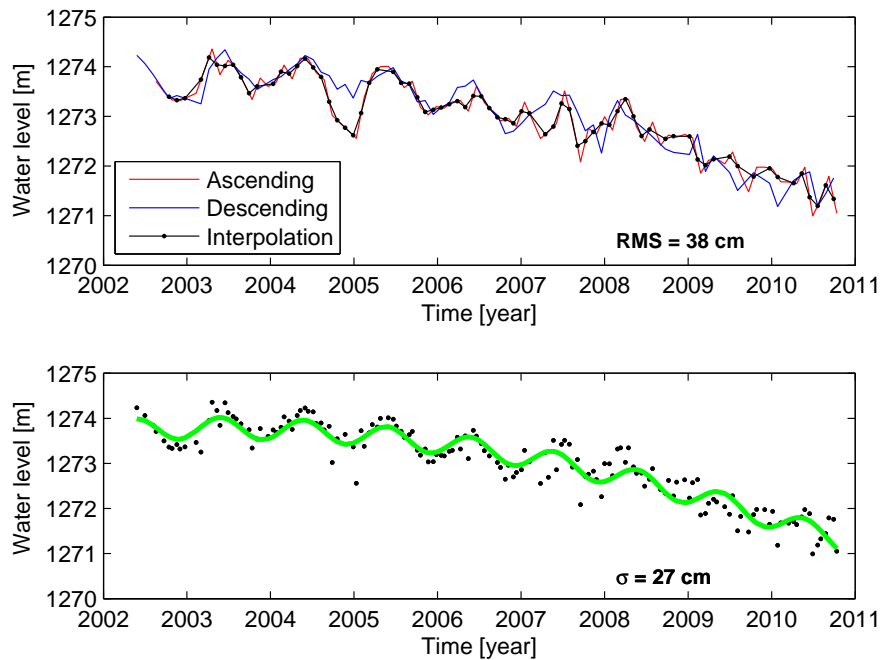
Figure 4.11: *Comparing water level from the ascending and descending tracks (upper panel), combined water level time series (lower panel) - from the MEDIAN values based on ice-1 retracker*
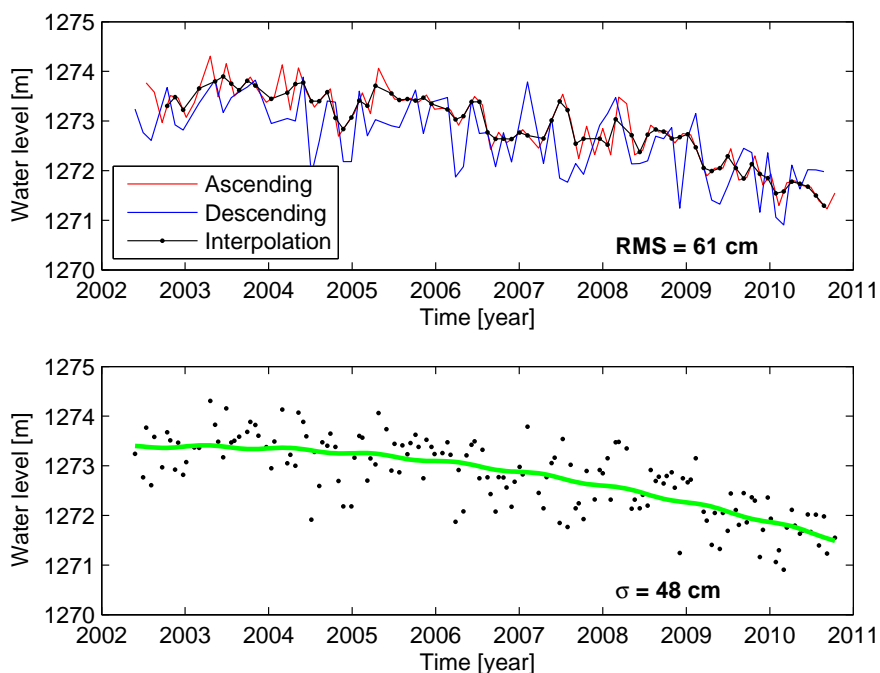
Figure 4.12: *Comparing water level from the ascending and descending tracks (upper panel), combined water level time series (lower panel) - from the MEAN values based on ice-1 retracker*

altimetry and in-situ gauge data. Here we plotted only the result from ice-1 retracker against in-situ gauge time series. From the external validation we found that there is no bias between water level from the altimetry and in-situ gauge for the tracker and retrackers. The water level from the ALL values has the maximum RMS and the water level from the MEDIAN values has the minimum RMS with respect to the in-situ gauge water level.

Table 4.6: *The water level RMS* (cm) *obtained from validation*

retracker	Internal			External		
	ALL	MEDIAN	MEAN	ALL	MEDIAN	MEAN
ice-1	90	**38**	61	53	**26**	47
ice-2	112	114	58	78	52	57
seaice	196	115	98	152	107	112
ocean	191	66	70	110	65	56

4.5 Assessment of water level time series from altimetry

A general comparison of water level from the ascending and descending tracks in figures 4.11 and 4.12 shows that they are consistent and there is not unusual change in terms of bias and

systematic error in the time series. Also from comparison of the combined water level from ascending/descending tracks with the in-situ gauge data (figure **??**), we found that there is no bias between water level from the satellite and in-situ gauge data. Because the in-situ gauge data is referenced to geoid EGM96 and this model of the geoid also is provided in GDR data of Envisat which we used in water level determination.

From figure 4.14 one can apparently see the annual periodic term of water level from the in-situ reading gauge. The annual behavior also can be seen from the altimetry time series especially for the water level from the MEDIAN values (figure 4.14 mid panel). Figure 4.14 clearly speaks that the water level from MEDIAN values follows the in-situ gauge water level better than that the MEAN and ALL values would do. Also comparing numerical result from external validation in table 4.6 shows that the MEDIAN values outperforms the ALL and MEAN value for all retrackers except than ocean tracker. The ocean is not reliable tracker for inland water bodies and this exception can not be a negative point against the performance of the MEDIAN values. As it is clear from the in-situ gauge time series (figure 4.13) the maximum water level recorded in 1995 about 1278 m that is a unique peak of water height during past 47 years.

Based on Envisat GDR data, lake water level has been steady declining since 2002 that confirmed by in-situ gauge reading, i.e. there is the same behavior for in-situ gauge time series during this time.

Comparing the result of our data analyzing from the ALL, MEDIAN and MEAN values of water level based on the tracker and different retrackers which are in table 4.6, confirms that using the MEDIAN values of water level for each satellite overpass based on retracker ice-1 provide the minimum values of standard deviation and RMS in the water level determination. Therefore using the MEDIAN operator and retracker ice-1 algorithm would be the most robust estimator to determine water level in the case of Urmia lake. So hereafter we only select the water level of the lake based on the MEDIAN values retracked by ice-1 algorithm to compare with the water level from other retracker algorithms which are described in chapter 5.
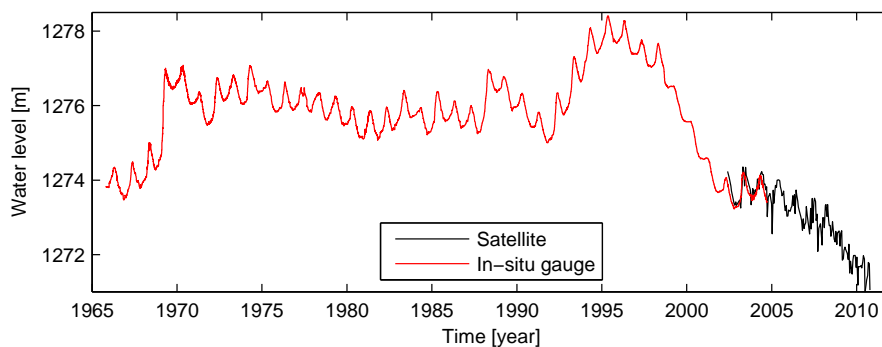

Figure 4.13: *Water level time series from satellite data (the MEDIAN values) based on ice-1 retracker and all in-situ gauge data*
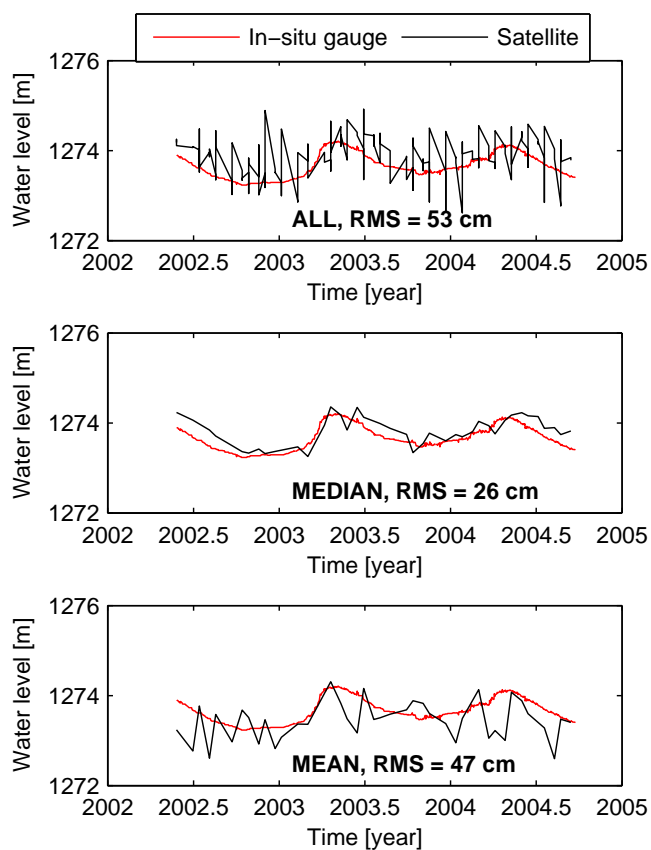
Figure 4.14: *Water level from in-situ gauge and satellite data based on ice-1 retracker from the ALL values (top), the MEDIAN values (mid) and the MEAN values (bottom)*

Chapter 5

Waveform retracking

Retracking means reprocessing and analysis of the altimetry waveform data to retrieve an optimized gate or bin for the range measurement. The general purpose of waveform retracking is to improve the quality of range measurements. Retracking also leads to improved estimation of parameters such as significant wave height and backscatter coefficient. It can increase the number of valid observations, particularly in coastal zones or over inland shallow water bodies (Anzenhofer et al., 1999). Near the lake shoreline or over shallow water the altimetry waveforms are generally contaminated by responses from non-water bodies inside the footprint of the radar. If the extracted ranges from these corrupted waveforms are used, water level monitoring will be corrupted as well. Extracting the right range from the corrupted waveform is a challenge over inland water bodies. Figure 5.1. and figure 5.2 show the complex situation of illuminated area by the radar pulse. Reflected signals are coming from the land and water surface (land contamination). From these figures we can see that reflected signals from the land causes unwanted peaks in the waveform that need to be taken care for precise water level determination. Retracking is the procedure to improve the range measurement from the measured waveforms. The quality of water level estimation depends on the type of retracking algorithms. Since there is no standard way to select a proper retracking for a given water body, we must test different retracking algorithms and examine their performance.

Figure 4.2 (lower panel) demonstrates the practical land contamination that caused such divergence in water level time series of Urmia lake. As mentioned in chapter 4, GDR data were processed using the on-board tracker and retrackers to define this time series. After all effort, i.e. estimation of the model (equation 4.1) via the least squares method in an iterative way and performing statistical tests to delete outliers, still we have a such water level time series that can not follow the real behavior of water level of the lake. Figure 4.1 (a) shows that the satellite descending passes are very close to the lake shoreline so the powers reflect from the land deteriorate the waveform and cause erroneous range measurements. Therefore, to obtain qualified water level time series, waveform retracking is necessary.
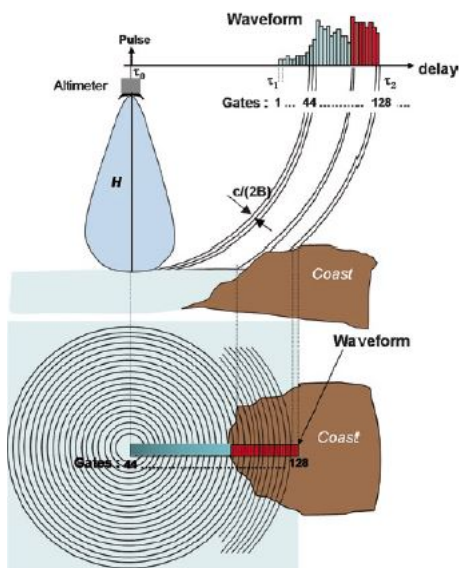
Figure 5.1: *Schematic representation of a transmitted pulse from the altimeter to the water surface in a coastal zone (top panel), Top-down view of the pulse limited footprint corresponding to each waveform. B is the bandwidth of the altimeter and c is the speed of light (lower panel) (Vignudelli et al., 2011).*
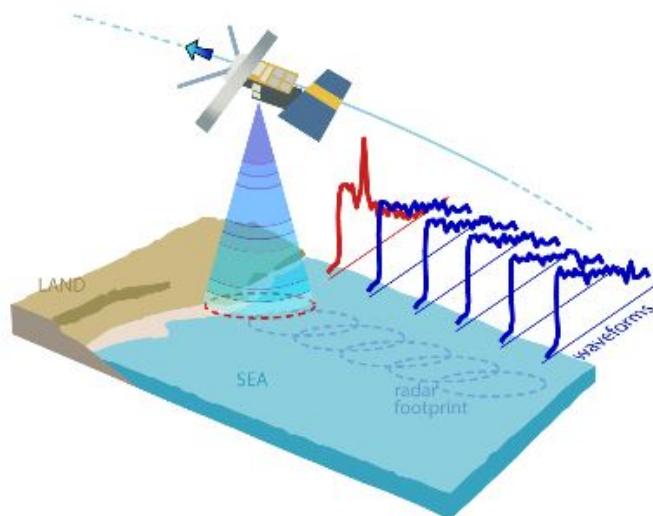
Figure 5.2: *Waveform contamination over shallow water or near the shoreline when the satellite is leaving or approaching the shoreline (http://www.aviso.oceanobs.com)*

5.1   Waveform retracking algorithms

A number of different waveform retracking algorithms to process altimetry waveforms exist. In this section we explain the retrackers that we used to process SGDR data of Envisat.

5.1.1 Offset Center of Gravity (OCOG)

The offset center of gravity retracking algorithm was developed by Wingham et al. (1986) to provide robust retracking algorithm. In this method the gravity center of the waveform is searched based on the power level of gates. In figure 5.3 the schematic diagram of this method is plotted. OCOG is a simple waveform retracker based on the statistic properties of the waveform.

It is very easy for OCOG to retrack the waveforms but its precision is generally low because this method is independent of physical characteristics of reflecting surfaces. OCOG is the algorithm behind ice-1 retracker on-board Envisat and sometimes it is used to calculate the initial values for other retracker algorithms. Based on the definition of a rectangle about the effective center of gravity of the waveform, we have the following formulas (Wingham et al., 1986):

$$A = \sqrt{\frac{\sum\limits_{i=1+n_1}^{N-n_2} P_i^4(t)}{\sum\limits_{i=1+n_1}^{N-n_2} P_i^2(t)}} \ , \tag{5.1}$$

$$W = \frac{\left(\sum\limits_{i=1+n_1}^{N-n_2} P_i^2(t)\right)^2}{\sum\limits_{1+n_1}^{N-n_2} P_i^4(t)} \ , \tag{5.2}$$

$$COG = \frac{\sum\limits_{i=1+n_1}^{N-n_2} i P_i^2(t)}{\sum\limits_{i=1+n_1}^{N-n_2} P_i^2(t)} \ . \tag{5.3}$$

In these equations A is the amplitude, W is the width and COG is the i-coordinate of the center of gravity of the waveform. P_i is the waveform power, N is the total number of samples in the waveform, $n_1 = n_2 = 4$ are the number of bins affected by aliasing at the beginning and end of the waveform. Finally the leading edge position (LEP) is:

$$LEP = COG - \frac{W}{2} \ . \tag{5.4}$$

5.1.2 Threshold

The threshold retracking method was developed by Davis (1995) to improve range estimation. In this method to determine the retracked gate, the dimensions of the rectangle defined by OCOG algorithm are used. Usually this retracker technique is used to retrack the waveforms over coastal zones and lakes (Davis, 1997). It is sensitive to the surface topography but is simple to implement. The threshold value is referenced with respect to the OCOG amplitude 10%, 20% and 50% (Guo et al., 2006). The retracked gate is determined by linear interpolation between neighboring gates of the threshold value crossing the leading edge of the waveform. The
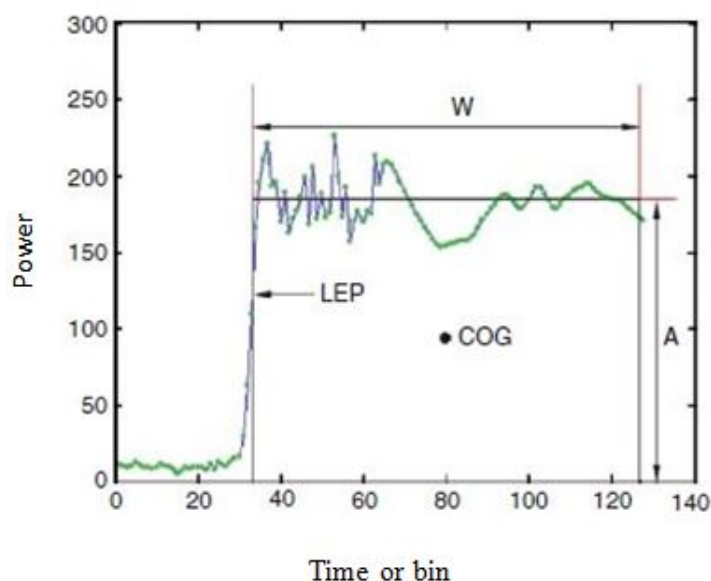
Figure 5.3: *Schematic diagram for OCOG retracker (Wingham et al., 1986)*

threshold method is also statistic and has no physical meaning. For volume scattering (reflection is caused by inclusion in the media) threshold level of 10-20% and for surface scattering 50% threshold level is used (Vignudelli et al., 2011). The retracked gate can be computed from the following equations:

$$P_N = \frac{1}{5} \sum_i^5 P_i \ , \tag{5.5}$$

$$T_h = P_N + q(A - P_N) \ , \tag{5.6}$$

$$G_r = G_{k-1} + \frac{T_h - P_{k-1}}{P_k - P_{k-1}} \ , \tag{5.7}$$

where A is computed from equation 5.1, P_N is thermal noise, q is the threshold value, e.g. 20%, G_k is the k-th gate, k is the first gate exceeding the threshold T_h and G_r is the retracked gate.

5.1.3 β-parameter

The β- parameter retracker was the first algorithm developed by Martin et al. (1983) from the National Aeronautics and Space Administration (NASA) to retrieve ranges from the SEASAT radar altimeter over continental ice sheets. This method uses a relevant parametric function to fit the altimeter waveform based on the Brown model. The ice altimetry group of the NASA's Goddard Space Flight Center (GSFC) has developed algorithms based on these function to retrack the ice sheet's waveform (Vignudelli et al., 2011). So this method of retracking is also known as NASA algorithm. It can be used as a 5β and 9β parameters to fit to single and double ramped waveforms respectively. A double ramped waveform can be considered as a

waveform that includes two sub-waveforms (the sub-waveform is explained in the following section). The general parameter function fitting model is given as follow ([Martin et al., 1983]):

$$y(t) = \beta_1 + \sum_{i=1}^{n} \beta_{2i}(1 + \beta_{5i}Q_iP\left(\frac{t - \beta_{3i}}{\beta_{4i}}\right) \quad , \tag{5.8}$$

in which:

$$Q = \begin{cases} t - (\beta_{3i} + 0.5\beta_{4i}) & \text{if} \quad t \geq \beta_{3i} + 0.5\beta_{4i} \\ \\ 0 & \text{if} \quad t < \beta_{3i} + 0.5\beta_{4i} \end{cases} \quad , \tag{5.9}$$

$$P(x) = \int_{-\infty}^{x} \frac{1}{\sqrt{2\pi}} \exp\left(\frac{-q^2}{2}\right) dq \quad . \tag{5.10}$$

n=1 or 2 stands for the number of the ramp in the waveform and the other parameters are:

- β_1: the thermal noise level of the returned waveform

- β_{2i}: the returned signal amplitude

- β_{3i}: the mid-point on the leading edge of the waveform (retracked gate)

- β_{4i}: the returned waveform risetime

- β_{5i}: the slope of the leading edge

These unknown parameters can be estimated by least squares method. Since equation 5.8 is non-linear it must be linearized. So we used linear least squares parametric adjustment (LLSPA) in an iterative way to estimate unknown parameters. Initial values were calculated from OCOG retracker.
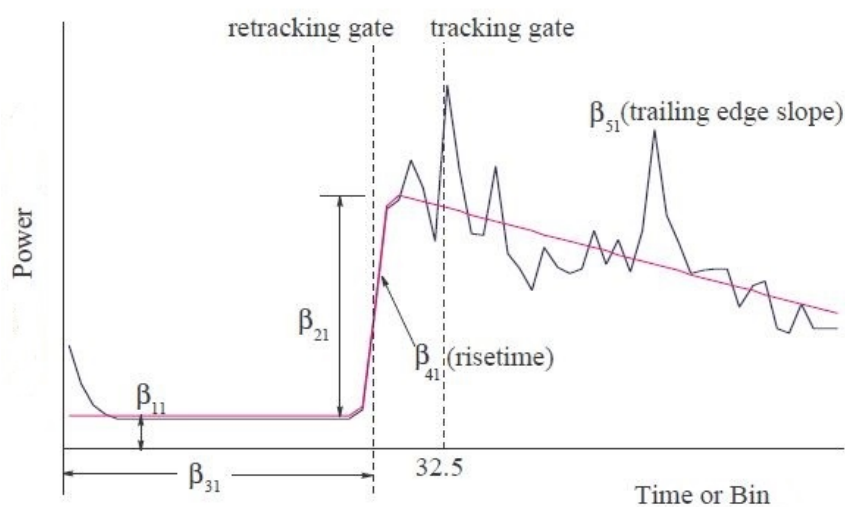

Figure 5.4: *5β parameters function fitting model fit to the single ramped waveform of ERS-1 ([Martin et al., 1983])*
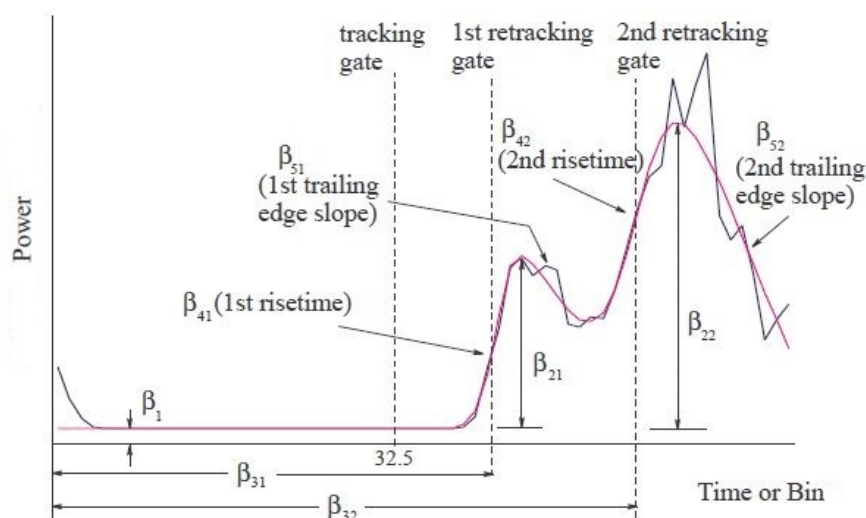
Figure 5.5: *9β parameters function fitting model fit to the double ramped waveform of ERS-1 (Martin et al., 1983)*

5.2 Sub-waveform retracking

Over the shallow water lake or near the shoreline waveforms are highly contaminated. Inside a given footprint of the radar there are different terrains, e.g. water, land and vegetation canopy, with different responses to the radar pulse that cause multiple meaningful peaks in the waveforms. Therefore returned waveforms can be considered as a combination of several small waveforms, called sub-waveforms (Guo et al., 2010a). Figure 5.6 shows a multi-peak waveform of Envisat that includes two sub-waveforms. An example of sub-waveform can be found in figure 5.7.

To each potentially meaningful peak a leading edge corresponds. For more precise ranging the leading edges need to be scrutinized. The idea of sub-waveform retracking was originally introduced by Guo et al. (2006) for recovery of gravity anomaly over coastal oceans. The goal of sub-waveform retracking technique is to find all potentially meaningful leading edges for further processing. After finding them, the sub-waveforms are modeled and retracked by one of the retrackers i.e. OCOG, threshold and β-parameter. Since sub-waveforms are single ramp waveforms, 9β parameters is not a proper retracker to retrack them instead 5β parameter retracker can be used.

Sub-waveform detection methodology

To detect potentially meaningful peaks, first the mean difference between the power at every gate and the gate after the next is computed:

$$d_2^i = \frac{1}{2}(P_{i+2} - P_i) \qquad \text{for Envisat}, i = 1, 2, ..., 126 \ . \tag{5.11}$$

P_i is the returned power for the i-th gate. While $d_2^i > \epsilon_2$, the index i is set to $i = i + 1$, until $d_2^{i+j-2} > \epsilon_2$ and $d_2^{i+j-1} \leq \epsilon_2$ with $j \geq 3$, now the leading edge has been found with a doubt. To find the real leading edge the power difference between the neighboring gates is computed:

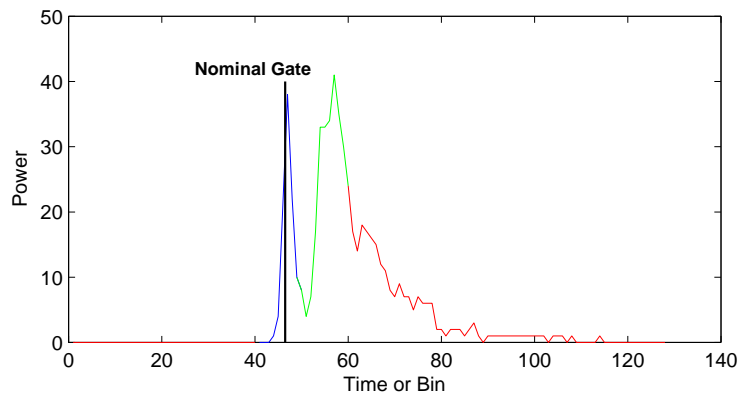**Figure 5.6:** *A full waveform of Envisat over Urmia lake (ascending pass #371, August 2005) includes 2 sub-waveforms*
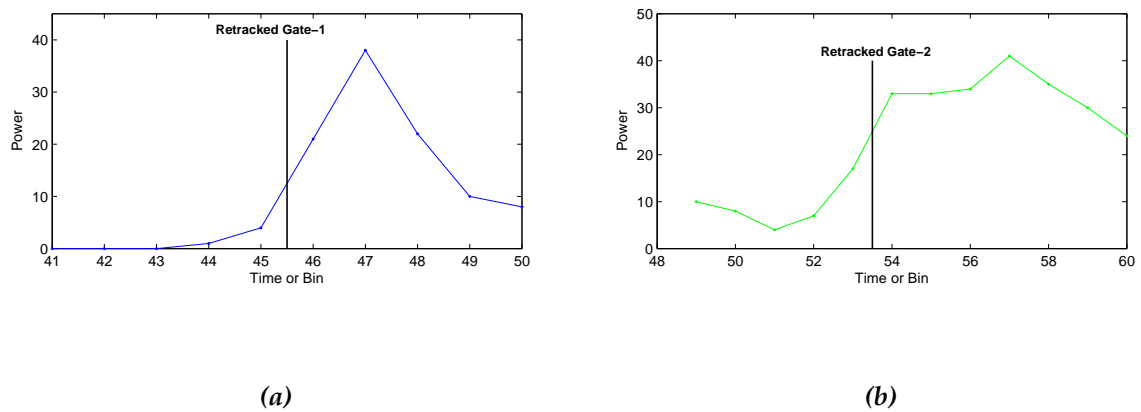

(a)   *(b)*

Figure 5.7: *Sub-waveforms extracted from the waveform in figure 5.6*

$$d_1^k = P_{k+1} - P_k, \qquad k = i, i+1, i+2, ..., i+j-2, i+j-1 \ , \tag{5.12}$$

If d_1^k is greater than a threshold value ϵ_1, the k-th gate included in the leading edge gates. If only one $d_1^k \leq \epsilon 1$ appears, it also belongs to the leading edge. Guo et al. (2006) and Guo et al. (2009) used fixed number for ϵ_1 and ϵ_2 but since over the shallow water waveforms have different shapes it is better to compute ϵ_1 and ϵ_2 according to the shape of the waveforms. Here we used $\epsilon_1 = 0.2S_1$ and $\epsilon_2 = 0.2S_2$ as used by Fenoglio et al. (2010).

After finding the leading edge n samples forward from the i-th gate and backward from $i + j - 1$-th gate, $P_k(k = i - n, i - n + 1, i - n + 2, ..., i - 1, i, ..., i + j - 2, i + j - 1, i + j, ..., i + j - 2 + n, i + j - 1 + n)$ are selected to form the sub-waveform. In general $n \leq 5$. S_1 and S_2 are computed from following equations:

$$S_1 = \sqrt{\frac{(N-1)\sum\limits_{i=1}^{N-1}(d_2^i)^2 - \left(\sum\limits_{i=1}^{N-2}d_2^i\right)^2}{(N-1)(N-2)}} \ , \tag{5.13}$$

$$S_2 = \sqrt{\frac{(N-2)\sum\limits_{i=1}^{N-2}(d_2^i)^2 - \left(\sum\limits_{i=1}^{N-2}d_2^i\right)^2}{(N-2)(N-3)}} \ , \tag{5.14}$$

where N is the number of gates in the waveform.

Detected sub-waveforms can be retracked by one of the retrackers, e.g. OCOG, Threshold and 5β parameters, to estimate retracked gate for correcting the range measurements.

5.3 Waveform modification

Over the coastal zones area or over the shallow water lake the responses from non-water surface (unwanted echo) make spurious peaks in the waveform and cause unusual behavior of the waveform in a few gates. These unwanted peaks due to environmental contamination can lead to outlying powers at few gates of the waveform. These outlying powers need to be modified to minimize the error in determination of the leading edge. Figure 5.8 shows an example of waveform modification over the coastal zone.

Also, sometimes due to instrumental problem of the radar system, waveforms can be affected by systematic error in a few gates. For example the waveform in figure 5.9 clearly has an outlying power at gate 61. The Range derived from such a waveform would not be proper range and maybe it would be a wrong range. In such a corrupted waveform the outlying powers can be modified based on the power of the same and adjacent waveforms. But if the systematic corruption happens in many gates then it would be better to delete the whole waveform.

Tseng et al. (2013) modified Envisat and Jason-2 altimeter waveforms and retracked them by different retrackers over the coastal zones in the north of America. Their result indicates that modified waveform retracking improves the accuracy of water level with respect to the original

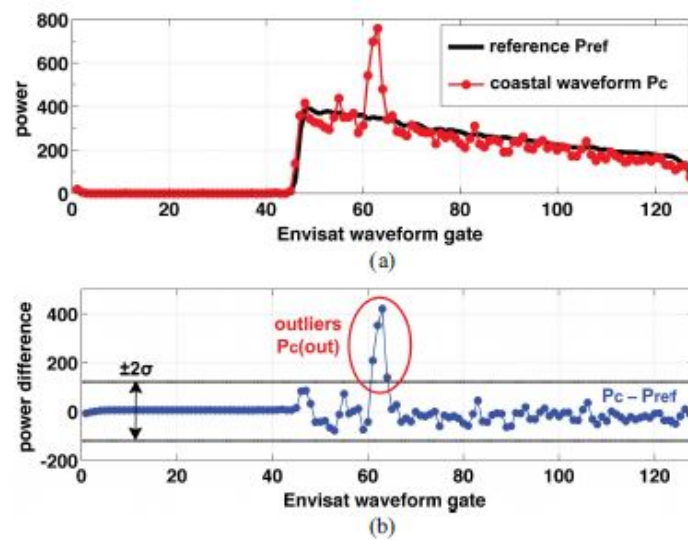**Figure 5.8:** *Detection the outlying powers in the coastal waveform of Envisat pass #305, cycle 92. (a) Contaminated waveform (red) compared with a reference waveform (black). (b) Powers difference exceeding ± 2 σ in the difference P- P_{ref} are considered as outliers (Tseng et al., 2013).*
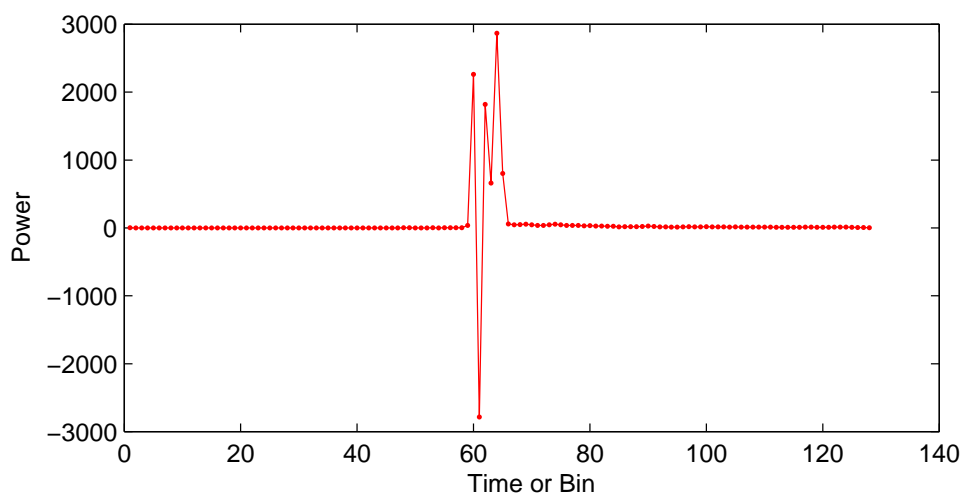

Figure 5.9: *A corrupted waveform of Envisat (ascending pass #178, May 2002) with outlying power in one gate*

waveform retracking by 63%. We tried to use this type of retracking in our area of study, Urmia lake. There are few number of waveforms (50 numbers from 2007 waveforms) what shown in figure 5.9, in our data set that need to be modified . Waveform modification requires a proper reference waveform to detect the outlying powers. Over the coastal zones it is easy to define the reference waveform. For a given satellite pass it can be defined by averaging the waveforms away from the coast. Tseng et al. (2013) averaged the waveforms 20–30 km from the coast in each cycle and used it as a reference waveform. The reference waveform P_{ref} is calculated as:

$$P_{\text{ref}}(i) = \frac{1}{k} \sum_{n=1}^{k} P(i), \qquad i = 1, 2, ..., 128 \ , \tag{5.15}$$

where k is the number of waveforms to be averaged and $P(i)$ is the power at i-th gate of the waveform. This waveform is subtracted from all original waveforms in the same pass to detect the outlying powers. If the power difference, $|P(i) - P_{\text{ref}}(i)|$, exceeds 2σ or 3σ (σ is the standard deviation of the power differences between a given waveform and the reference waveform), the power is considered as an outlier that must be deleted from the waveform. Deleted powers are replaced by interpolation, based on the power of neighboring gates in the same waveform and the power of the same gates and neighboring gates in the adjacent waveforms. Following equation used by Tseng et al. (2013) to replace the deleted powers:

$$\bar{P}(j) = \frac{1}{2\sqrt{2}+4} \left\{ [P(j+1) + P(j-1) + P_{+1}(j) + P_{-1}(j)] + ... \right.$$
$$\left. \frac{1}{\sqrt{2}} [P_{+1}(j+1) + P_{-1}(j-1) + P_{+1}(j-1) + P_{-1}(j+1)] \right\} \ , \tag{5.16}$$

in which $\bar{P}(j)$ is the patched power for the outlying j-th gate, P_{-1} and P_{+1} are the powers of the adjacent waveforms.

Over a shallow inland water body like Urmia lake the waveform shapes are so diverse, even for a given pass that we can not define a proper reference waveform. Figures 5.10 and 5.11 show waveform variations along a descending track of Envisat over this lake. As we can see from these figures, due to variety of waveform variations in a given pass defining a proper reference waveform is too difficult or it is impossible. For this lake there is a big difference between the reference waveform and a given waveform of the same pass. The reference waveform (green curves) in figure 6.8 is the average of 320 waveforms in a given pass. In this figure the standard deviation of power differences between the reference waveform and other waveforms varies from 657 to 6927 w, that are big values with respect to the power of waveforms. So it is not clear what the outlying powers are. That means modifying waveforms over the shallow water body like Urmia has too much limitations. Therefore we could only detect such a clear outlying power in figure 5.9, the powers with negative values.
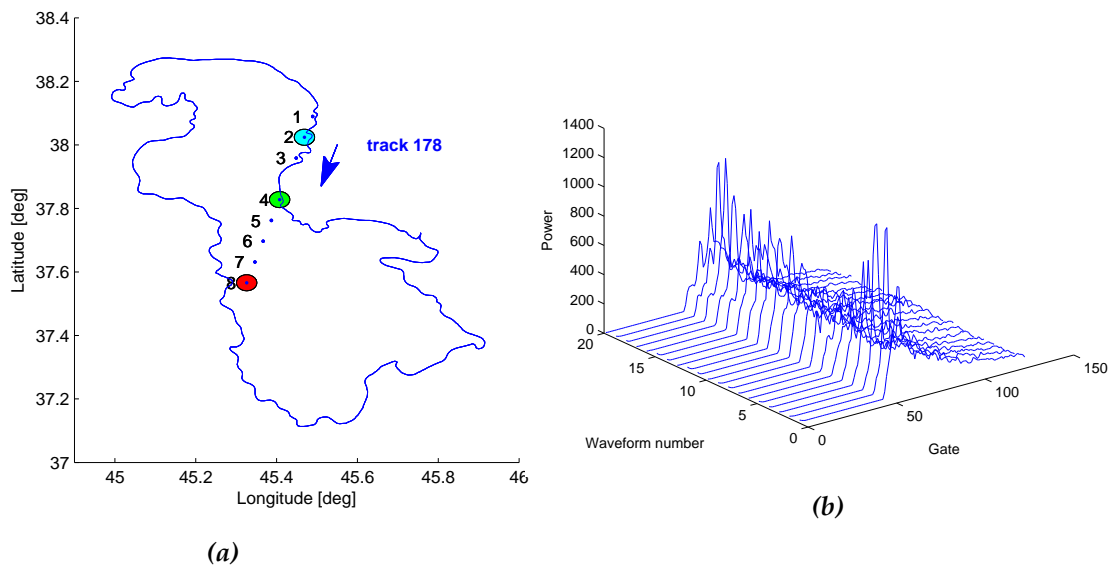
(a)

(b)

Figure 5.10: *Sub-satellite points of Envisat over Urmia lake (a) and Waveform variations for location 2 of descending pass 178, May 2002 (b)*
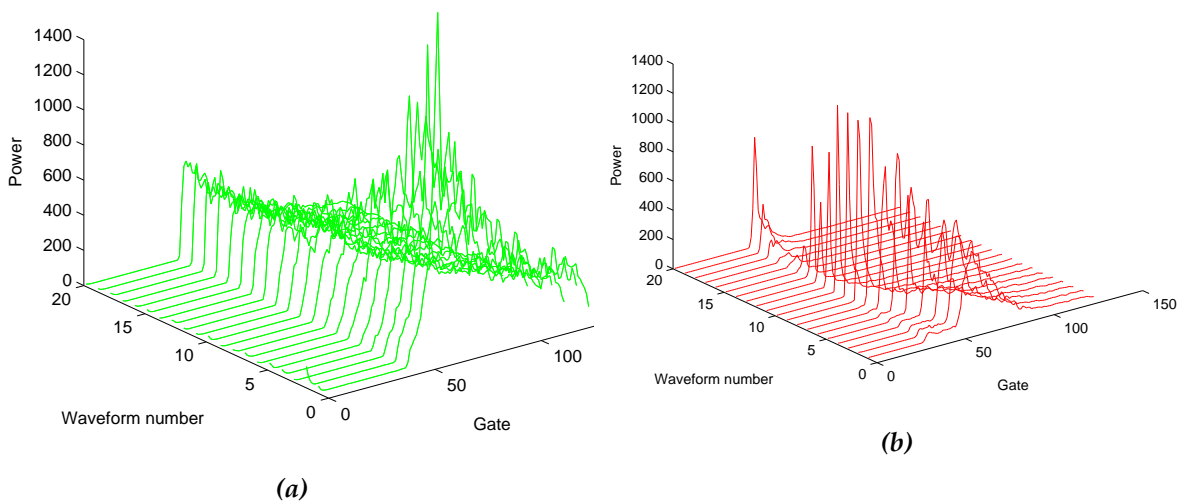

(a)

(b)

Figure 5.11: *Waveform variations for location 4 (a) and location 8 (b) of descending pass 178, May 2002*

Chapter 6

Retracked water level

In this chapter we estimate the water level of Urmia lake from Envisat SGDR data according to the retracking scenarios described in chapter 5 and summarized in figure 6.1. The retracked gate was estimated from all retrackers and used to calculate range correction by:

$$\Delta R_{\text{Ret}} = (\text{Gate}_{\text{Ret}} - \text{Gate}_{\text{Nom}})\tau\frac{c}{2} \; , \tag{6.1}$$

where Gate_{Ret} is the retracked gate estimated from one of the retracking techniques and Gate_{Nom} is the nominal tracking gate that we know from the satellite handbook, i.e. 46.5 for Envisat. τ is the pulse duration known from the satellite manual: it is 3.125 ns for K-band signal of the radar mounted on Envisat satellite (http://earth.esa.int/pub/ESA_doc/Envisat/RA2/) and c is the light velocity in vacuum. To determine retracked water level, equation 2.13 was modified by adding ΔR_{Ret} to R. R is extracted from GDR data and corrected for media and geophysical corrections which are included in GDR data.

We retracked the water level of the lake based on different retracking algorithms and plotted the result in figures 6.2 – 6.7. Table 6.1 shows the mean and standard deviation of ΔR_{Ret} for all satellite passes based on different retracking scenarios for the original waveforms.

In chapter 4 we derived water level time series of the lake according to the on-board tracker and retrackers for ascending and descending tracks separately. We found that there is no bias and systematic error between water level from ascending and descending tracks. Therefore we didn't perform retracking analysis separately for the ascending and descending tracks in this chapter. But after retracking, these separated time series were combined to build up a united water level time series. The same model, as what we used for the on-board tracker and retrackers, i.e. equation 4.1, was used to detect and eliminate outliers. It is worthy to mention that this model (trend) is just a means to quantify the error level of the retrackers internally.

To retrack water level variations, first we retracked the original waveforms. Then waveforms were modified and retracked again. In both cases (original and modified), waveforms were considered as full and sub-waveforms. In the full-waveform retracking we retracked a given waveform as one waveform and we estimated one corrected range per waveform. But in the sub-waveform retracking we assumed that a given waveform is a combination of few number of small waveforms, called sub-waveforms. The sub-waveforms inside a waveform were retracked separately. From each sub-waveform one retracked range correction was estimated.
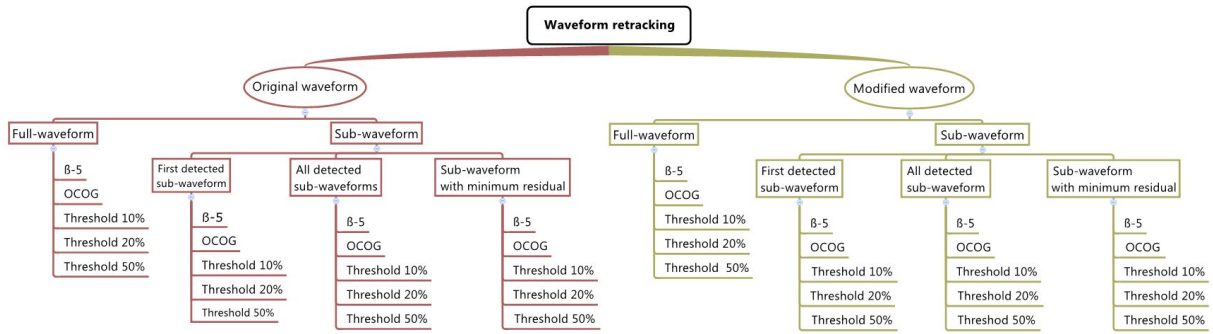
Figure 6.1: *Retracking scenarios*

Table 6.1: *Mean* (m)/ *standard deviation* (m) *of* ΔR_{Ret} *for all of the original waveform retracking scenarios in figure* 6.1

retracker	full-waveform	sub-waveform		
		first	mean-all	min-residual
β-5 parameter	7.84/4.41	20.32/0.70	20.85/0.80	20.67/0.90
OCOG	2.64/1.22	19.50/0.49	20.39/0.75	20.86/0.84
Threshold 10%	2.75/0.81	19.83/0.14	19.16/0.21	19.99/0.22
Threshold 20%	2.60/0.86	19.73/0.22	19.85/0.26	19.94/0.26
Threshold 50%	2.54/1.38	19.50/0.45	19.67/0.39	19.81/0.40

6.1 Water level from retracking the original waveforms

6.1.1 Water level from retracking the full-waveforms

The leading edge position computed from OCOG retracker (equation 5.4 was substituted in equation 6.1 to correct the extracted ranges from GDR data. After this correction we estimated water level of the lake, called retracked water level that shown in figure 6.2.

The retracked water level has a standard deviation of 27 cm, the same as what was obtained from on-board retracker, ice-1. From figures 6.2 and 4.11 we can see that there is no improvement (in terms of standard deviation of the residual) in water level determination by OCOG retracker respect to the on-board retracker in the case of Urmia lake if we do the full-waveform retracking. Since for retracking we need extra computations which is time consuming, there is no benefit to employ OCOG retracker technique in the full-waveform retracking. It is better to use ice-1 instead.

Threshold retracker was developed to provide altimetry data over the ice sheet (Partington et al., 1989). It is sensitive to the surface topography and is simple to implement. Furthermore if the threshold level is chosen appropriately, it can provide accurate water level measurements (Davis, 1997). The retracked gate, Gate$_{\text{Ret}}$ computed based on this retracker was converted to the retracked range to estimate water level of the lake. Unlike OCOG, threshold retracker is working well to monitor water level of Urmia lake. In this study we examine threshold retracker with threshold values, 10%, 20% (for volume scattering) and 50% (for surface scattering). As we see from figure 6.3 the model fits to the retracked water level time series quite well.
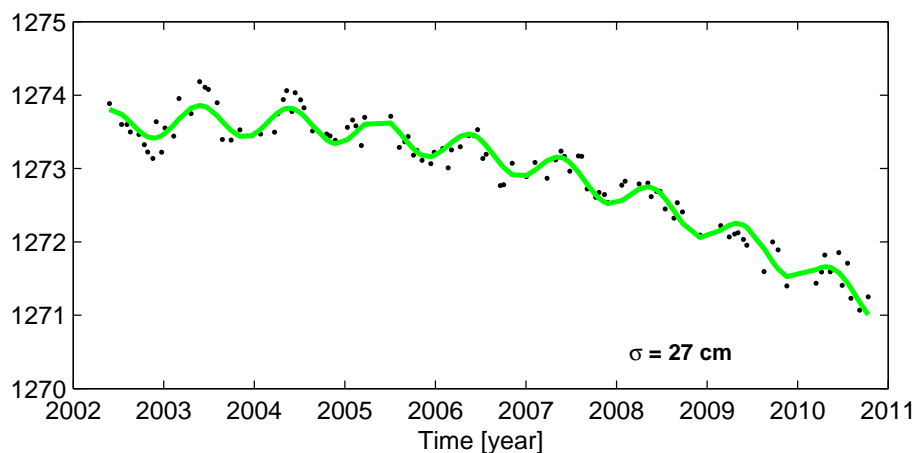
Figure 6.2: *Retracked water level from OCOG retracker using the full-waveform*

The standard deviation of water level time series are 18 cm, 15 cm and 17 cm for 10%, 20% and 50%, respectively. So this retracker outperforms the on-board and OCOG retrackers.

In our analysis we used 5β parameter retracker that can retrack both sub-waveform and full-waveform. β_{3i} in equation 5.8, estimated from LLSPA method, is the retracked gate. Figure 6.4 shows the water level of the lake retracked by 5β retracker. From this figure we can clearly see that the water level time series has poor quality if we employ this retracker. The standard deviation of water level is 70 cm. That is bigger than that obtained from the on-board retrackers, i.e. this technique is not suitable to retrack the full-waveform to determine water level of the lake.

6.1.2 Water level from retracking the sub-waveforms

In this approach of retracking all detected meaningful sub-waveforms were retracked by all of the retrackers, to find out the best retrackering scenario for water level monitoring of the lake. From a given sub-waveform one retracked gate is extracted. Therefore for a given waveform more than one range correction can be estimated. We must investigate to select the optimized one, which belongs to the water surface at nadir, to retrack the water level. The optimized sub-waveform is what produces the minimum RMS value in the water level determination when it is compared to in-situ gauge data. The sub-waveform was analyzed based on the following strategies to select the optimized one for retracking:

- Retracking the first sub-waveform

  We assume that the first sub-waveform is the response form the water surface at nadir location. So for all of the waveforms only the first detected sub-waveform has been considered to estimate retracked range correction. Consequently this sub-waveform was processed to retrack water level of the lake using all retracker algorithms. Having considered the first sub-waveform in the retracking, we found out that threshold 20% retracker
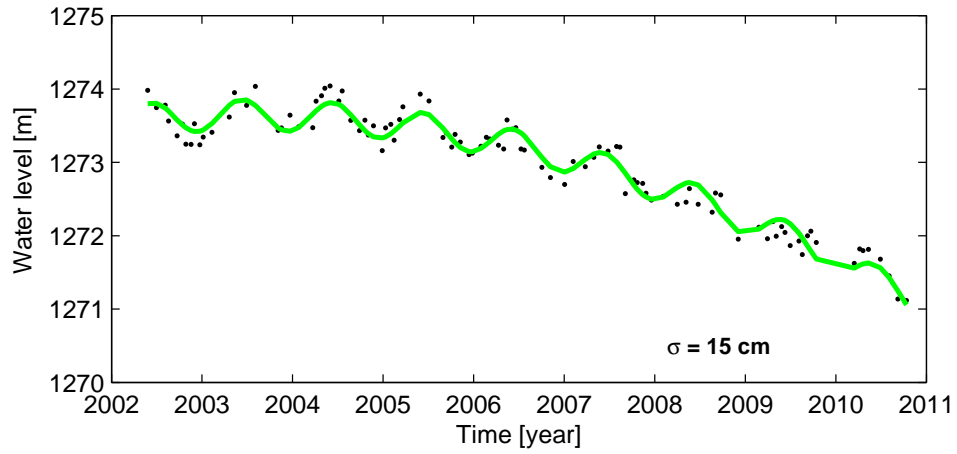
Figure 6.3: *Retracked water level from threshold 20% retracker using the full-waveform*
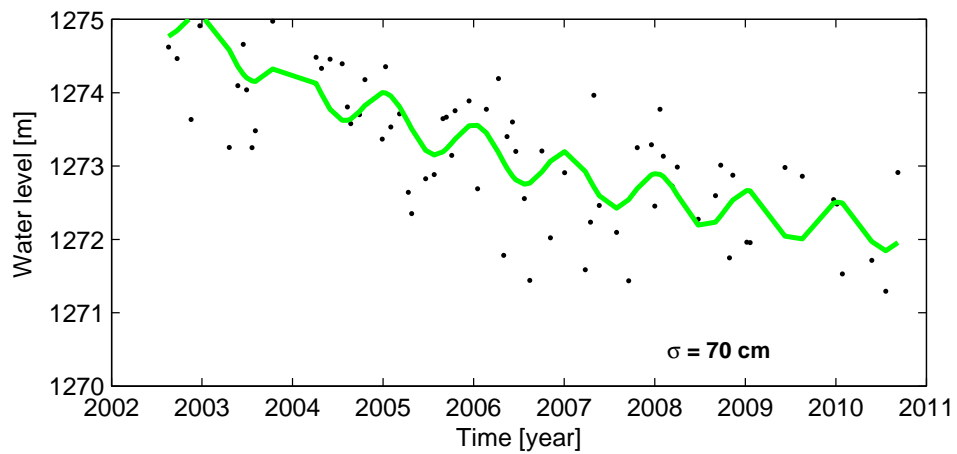

Figure 6.4: *Retracked water level from 5β retracker using the full-waveform*

provides the minimum standard deviation, i.e. 12 cm and 24 cm RMS (with respect to the in-situ gauge data) in retracking water level of the lake. Threshold 50% provides the minimum RMS value, 18 cm, and the standard deviation equals to 13 cm.
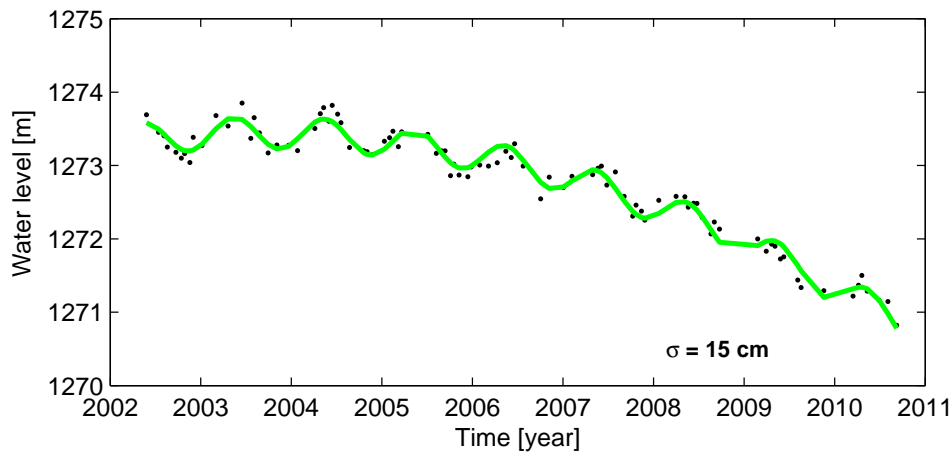

Figure 6.5: Retracked water level from threshold 20% retracker using the first sub-waveform

- Retracking all sub-waveforms

  In this method of sub-waveform retracking we don't know which sub-waveform belongs to the water surface at nadir. So for a given full-waveform we use all detected sub-waveforms to compute range correction. The final range correction is the mean value of the range corrections from all sub-waveforms included in the given full-waveform. For example the full waveform in figure 5.6 includes 2 sub-waveforms that shown in figure 5.7. So we have 2 range corrections ΔR_1 and ΔR_2. The mean value of ΔR_1 and ΔR_2 is the representative range correction for the whole waveform. In this type of sub-waveform retracking, threshold 10% has the minimum standard deviation, 14 cm, and 26 cm RMS. But threshold 50% produces the minimum RMS, 23 cm, with the standard deviation of 16 cm.

- Retracking a sub-waveform that provides the retracked water level with the minimum standard deviation

  In this analysis, we think that the optimized sub-waveform provides the minimum standard deviation for the water level. To find it, for a given full-waveform, the retracked water height was estimated from each sub-waveform. Then a sub-waveform which corresponds to the minimum standard deviation was selected to retrack the water level of the lake. Retracker threshold 10% provides the minimum standard deviation, 10 cm, with 25 cm of RMS.

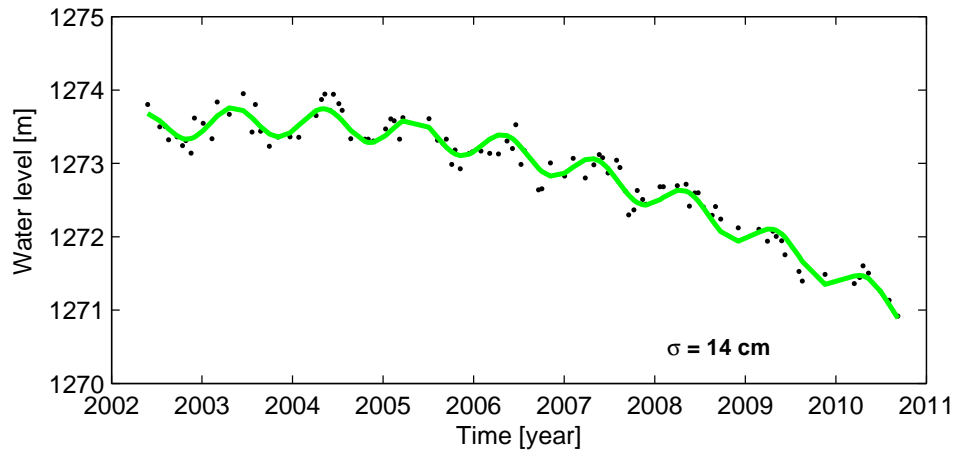***Figure 6.6:*** *Retracked water level from threshold 10% retracker using all sub-waveforms*
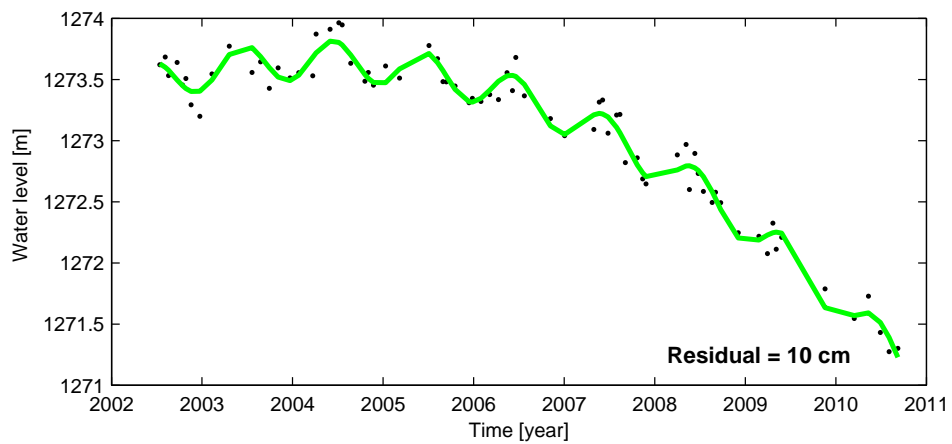

Figure 6.7: *Retracked water level from threshold 10% retracker using the sub-waveform that produces the water level with the minimum standard deviation*

6.2 Water level from retracking the modified waveforms

The majority of modification is due to land and environmental effects on the waveform (Tseng et al., 2013). On the other hand the reference waveform is fundamental for waveform modification. As mentioned before for the inland water body like Urmia lake defining the reference waveform is limited due to variety of waveform variations for a given satellite pass. Without a proper reference waveform it is not possible to modify the waveforms for environmental contaminations. As an example, we compared one part of the waveforms of a given pass of Envisat over Urmia lake with the reference waveform, defined from the same pass, in figure 6.8. In this figure red curves are the original waveforms and green curve is the reference waveform which is the averaged waveform for this pass. It is clear from this figure that there is a big difference between the reference waveform and a given waveform. So we can not detect outliers to modify the original waveforms.

Despite modification due to the land contamination, waveforms need to be modified because of systematic errors. Figure 5.9 shows a corrupted waveform with a negative returned power in one gate that is an outlier in the waveform. This waveform has been modified and plotted in figure 6.9. For precise and accurate water level measurements such an outlier must be removed and retrieved in a proper way. Over Urmia lake there are few number of such waveforms (50 from 2007 waveforms) which need to be modified. These waveforms after the modification were processed by different retrackers. Since there are only few number of such corrupted waveforms there was a small modification. Modified waveforms were retracked to determine water level of the lake. We found out that there is no improvement with respect to the retracking of the original waveforms. So modified waveform retracking algorithm was excluded from further processing and we stayed only on original waveform retracking, called waveform retracking.

6.3 Validation of retracked water level

The performance of the retrackers that used in this study to retrack the water level of the lake was assessed in two ways:
1- Internal validation
In this way, our judgment is based on the standard deviation of retracked water level time series after removing the model (equation 4.1). The model was fitted to the time series using LLSPA method in an iterative way to detect and delete the outliers. Finally the standard deviation was estimated for all retrackes that have been summarized in table 6.2.
2- External validation
In this comparison we assessed the accuracy of water level determination. To do that, the retracked water level time series from the satellite were compared with the water level defined from available in-situ gauge data. There is a bias between the retracked water level series and in-situ gauge data. The bias depends on the retracking algorithm and it was calculated form the difference of the mean retracked water level and the mean water level form in-situ gauge data. Table 6.3 shows the bias for all of the retrackers. In the full-waveform retracking all of the powers (except than few power at the beginning and end of the waveform due to aliasing effect) are used to estimate the corrected range while in the sub-waveform retracking only few powers with higher values are used that leads to bigger values for retracked range corrections
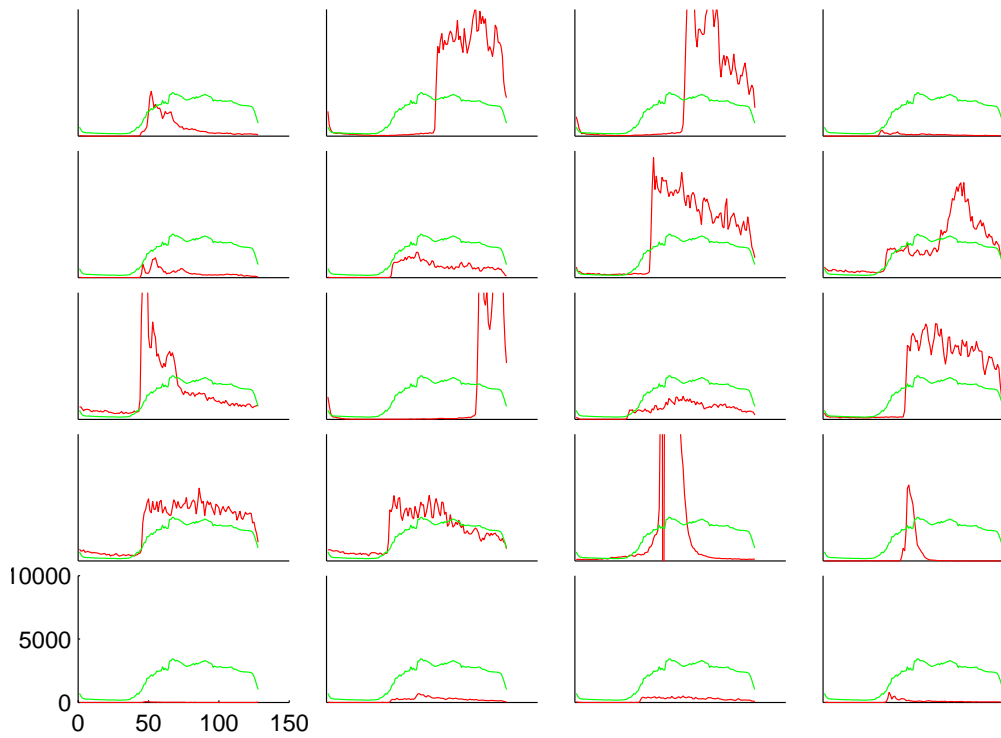
Figure 6.8: *The original waveforms (red) and the reference waveform (green) for one part of the ascending pass 371, May 2002*
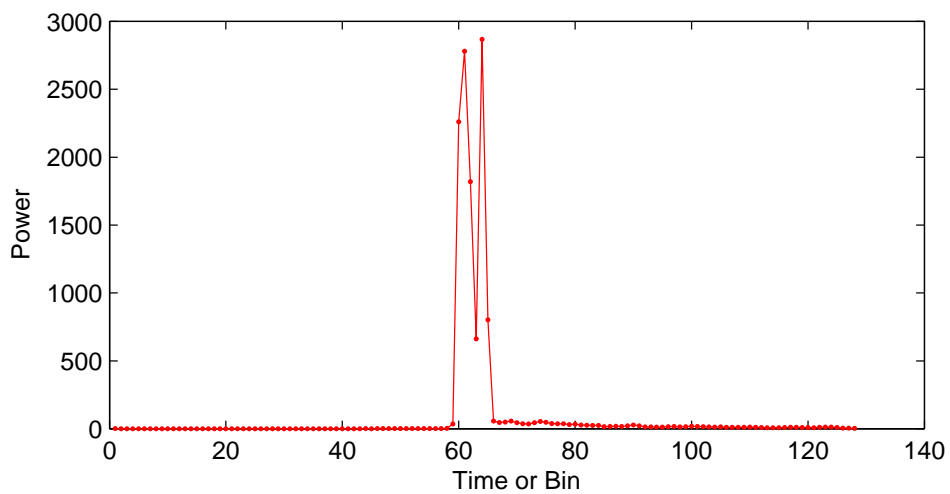

Figure 6.9: *Modified waveform of corrupted waveform in figure 5.9*

Table 6.2: Standard deviation (cm) *of the residual from different retrackers*

retracker	full-waveform	sub-waveform		
		first	mean-all	min-residual
Ice-1	27	–	–	–
β-5 parameter	63	22	20	20
OCOG	27	20	16	16
Threshold 10%	18	15	14	**10**
Threshold 20%	15	12	15	17
Threshold 50%	17	13	16	18

Table 6.3: Retracked water level bias (m) *with respect to the in-situ gauge data*

retracker	full-waveform	sub-waveform		
		first	mean-all	min-residual
Ice-1	0	–	–	–
β-5 parameter	2.17	19.51	21.48	21.43
OCOG	1.30	19.51	20.02	21.56
Threshold 10%	2.47	19.85	20.02	20.58
Threshold 20%	2.30	19.77	20.02	20.24
Threshold 50%	1.94	19.48	19.88	20.21

from the sub-waveform retracking. Consequently the biases of retracked water level from sub-waveform retracking are bigger than those from the full-waveform retracking. After removing the bias, retracked water level time series were compared again to the water level time series from the in-situ gauge data. The result of this comparison, in terms of RMS, is shown in table 6.4.

Table 6.4: Water level RMS (cm) *from different retrackers*

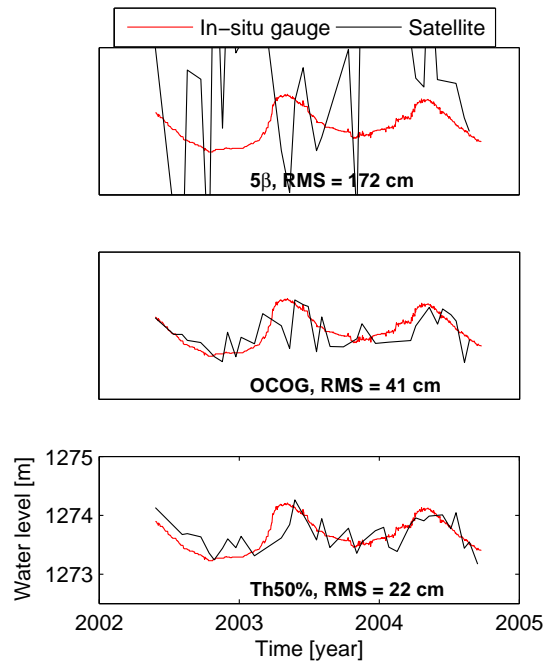| retracker	full-waveform	sub-waveform		
		first	mean-all	min-residual
Ice-1	26	–	–	–
β-5 parameter	172	22	36	38
OCOG	41	22	36	25
Threshold 10%	23	24	26	25
Threshold 20%	23	24	27	28
Threshold 50%	22	**18**	23	29

Figure 6.10: *Validation of retracked water level derived from retracking of the full-waveform*
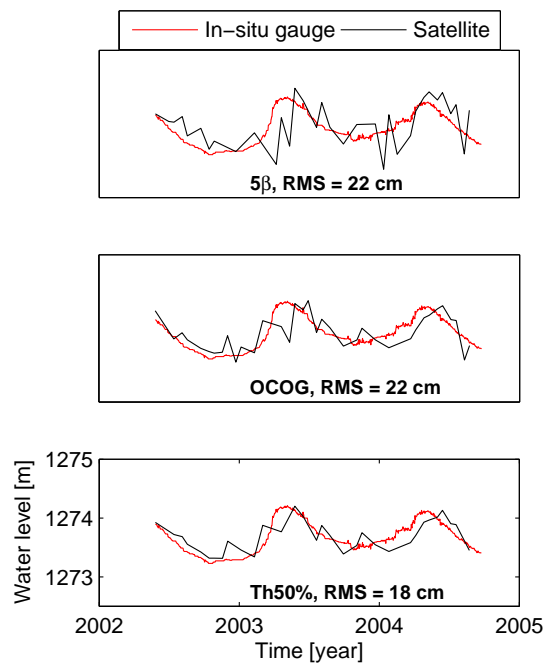

Figure 6.11: *Validation of retracked water level derived from retracking of the first sub-waveform*

Chapter 7

Discussion and conclusion

Defining water level time series separately for ascending and descending tracks based on the ALL, MEDIAN and MEAN values helps us to detect such an unusual behavior of water level shown in figure 4.2 (lower panel). This event was detected when water level was defined from the ALL values. This figure clearly speaks that close to the shoreline, on-board tracker and on-board retrackers can not provide the qualified (precise) water level time series. To avoid such an unusual event in figure 4.2 (lower panel) we had to delete one part of descending track data, that is not always a good solution. Because we lose data which are not necessarily unqualified data. Finally after removing one part of data, we found out that using the MEDIAN values and ice-1 retracker is the best retracking scenario to retrack water level of the lake if we only consider on-board tracker and retrackers. The water level RMS of 26 cm (figure 4.14, mid panel) has been obtained from this scenario.
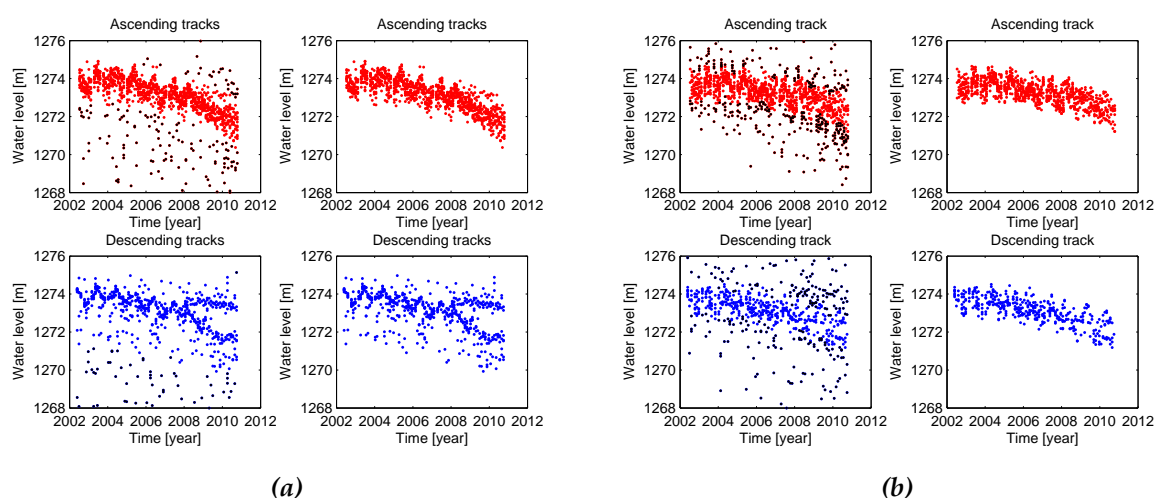
Figure 7.1: *Water level time series before waveform retracking (a) and after waveform retracking (b)*

A general comparison of figures 7.1-a and -b discloses the advantage of waveform retracking. With waveform retracking one can keep all of the measurements (except than outliers), even closed to the shoreline, to estimate water level variations. So there is more data available that can lead to a better estimation for water level of the lake.

The quality of water level time series depends on the retracking algorithm used to process the waveforms. Due to environmental effects on the waveforms, it is too difficult to define a standard waveform retracker for an inland water body like Urmia lake. We employed different retracker algorithms in the full and sub-waveform analysis to reduce the environmental

contamination and to improve the water level quality of the lake. The numerical result of the waveform retracking are summarized in tables 6.2 and 6.4. We validated the water level derived from satellite altimetry internally and externally.

The internal validation was performed in front of the model (equation 4.1) and comparing the water level from ascending/descending tracks. It shows that there is no bias and systematic error between ascending and descending track observations. The internal validation relates to the standard deviation and precision of water level. We have shown in chapter 4, ice-1 is the most precise and accurate retracker among on-board tracker and retrackers. It provides the standard deviation of 27 cm for water level of the lake. While the standard deviation from threshold 20% is 15 cm if we retrack the full-waveforms. If we retrack the sub-waveforms with threshold 10% retracker, shown in figure 6.7, the water level standard deviation is 10 cm that is a significant improvement. So internal validation indicates that threshold retracking algorithm with different threshold values has better performance to reduce the standard deviation of water level than the other retrackers would do. But only internal validation is not enough and we must do external validation too.

For the external validation we compared retracked water level derived from the satellite data to the water level from available in-situ gauge data. Table 6.4 shows that for the full-waveform retracking only threshold retracker improves the water level quality with respect to ice-1 retracker (the best on-board retracker). The maximum improvement is 4 cm which is achieved by threshold 50%. For 5β parameter retracker the accuracy before retracking is much better than that after retracking that means for the full-waveforms 5β parameter is not a proper retracker in the case of Urmia lake. But for the sub-waveforms, 5β parameter retracker shows a better performance to retrack water level of the lake. The accuracy of 22 cm has been obtained by this retracker when the first detected sub-waveforms in the waveform is retracked.

We analyzed all of the detected sub-waveforms to select the optimized one to be retracked. Our analysis has been performed in front of OCOG, Threshold and 5β parameter retrackers. First, we retracked the first detected sub-waveform for all of the waveforms. Second, for a given waveform all detected sub-waveform were retracked. In this case the final retracked range correction is the mean value of all retracked range corrections. Third, among all sub-waveforms of a given waveform the sub-waveform which provides the minimum standard deviation, for the water level, was retracked. The numerical result in table 6.4 indicates that the first detected sub-waveform in a given waveform is the optimized one to be retracked. Retracking over the first sub-waveforms via all retracker algorithms provides more accurate water level than that would obtain by on-board retrackers.

Generally we have improvement by all retrackers when the first sub-waveforms are retracked. The minimum RMS or the maximum accuracy (with respect to the in-situ gauge data), 18 cm, has been estimated by threshold 50% retracker. That means we have 8 cm improvement with respect to on-board retracker, ice-1. Therefore the first sub-waveform retracked by threshold 50% is the most accurate estimator to monitor the water level of Urmia lake.

Bibliography

Altés, AB, Cornara, FP and Renard, M (2010). *Next Generation Gravity Mission (NGGM): Mission analysis report*. Tech. rep., NGGM-DEM-TEC-TNO-01, Deimos.

Anzenhofer, M, Shum, CK and Rentsh, M (1999). *Coastal altimetry and applications*. Tech. rep., Report No, 464, Ohio State University.

Asem, A, Mohebbi, F and Ahmadi, R (2012). Drought in Urmia lake, the largest natural habitat of brine shrimp Artemia. *World Aquaculture*, **43**(1):36–38.

Biancamaria, S, Andreadis, KM, Durand, M, Clark, EA et al. (2010). Preliminary characterization of SWOT hydrology error budget and global capabilities. *Selected Topics in Applied Earth Observations and Remote Sensing, IEEE Journal of*, **3**(1):6–19. doi:10.1109/JSTARS.2009.2034614.

Brown, G (1977). The average impulse response of a rough surface and its applications. *Antennas and Propagation, IEEE Transactions on*, **25**(1):67–74. doi:10.1109/TAP.1977.1141536.

Davis, CH (1995). Growth of the Greenland ice sheet: a performance assessment of altimeter retracking algorithms. *Geoscience and Remote Sensing, IEEE Transactions on*, **33**(5):1108–1116. doi:10.1109/36.469474.

——— (1997). A robust threshold retracking algorithm for measuring ice-sheet surface elevation change from satellite radar altimeters. *Geoscience and Remote Sensing, IEEE Transactions on*, **35**(4):974–979. doi:10.1109/36.602540.

Deng, X (2003). *Improvement of geodetic parameter estimation in coastal regions from satellite radar altimetry*. Ph.D. thesis, Curtin University of Technology.

Fenoglio, ML, Fehlau, M, Ferri, L, Becker, M et al. (2010). Coastal sea surface heights from improved altimeter data in the Mediterranean sea. *Gravity, geoid and Earth observation, Springer Berlin Heidelberg*, pp. 253–261. doi:10.1007/978-3-642-10634-7_33.

Frappart, F, Calmant, S, Cauhopé, M, Seyler, F et al. (2006). Preliminary results of Envisat RA-2-derived water levels validation over the Amazon basin. *Remote Sensing of Environment*, **100**(2):252–264. doi:10.1016/j.rse.2005.10.027.

Fu, LL and Cazenave, A (2001). *Satellite altimetry and earth sciences a hand book of techniques and applications*. Academic press, San Diego, California.

Guo, JY, Chang, XT, Gao, YG, Sun, J et al. (2009). Lake level variations monitored with satellite altimetry waveform retracking. *Selected Topics in Applied Earth Observations and Remote Sensing, IEEE Journal of*, **2**(2):80–86. doi:10.1109/JSTARS.2009.2021673.

Guo, JY, Gao, YG, Chang, XT and Hwang, CW (2010a). Optimized threshold algorithm of Envisat waveform retracking over coastal sea. *Chinese Journal of Geophysics*, **53**(2):231–239. doi:10.1002/cjg2.1490.

Guo, JY, Hwang, CW, Chang, XT and Liu, Y (2006). Improved threshold retracker for satellite altimeter waveform retracking over coastal sea. *Progress in Natural Science*, **16**(7):732–738. doi:10.1080/10020070612330061.

Hayne, G, Hancock, D, Purdy, C and Callahan, P (1994). The corrections for significant wave height and attitude effects in the TOPEX radar altimeter. *Journal of Geophysical Research: Oceans*, **99**(C12):24,941–24,955. doi:10.1029/94JC01777.

Hwang, C, Peng, MF, Ning, J, Luo, J et al. (2005). Lake level variations in china from topex/poseidon altimetry: data quality assessment and links to precipitation and enso. *Geophysical Journal International*, **161**(1):1–11. doi:10.1111/j.1365-246X.2005.02518.x.

Jain, M, Andersen, OB, Dall, J and Stenseng, L (2015). Sea surface height determination in the arctic using CryoSat-2 SAR data from primary peak empirical retrackers. *Advances in Space Research*, **55**(1):40–50. doi:10.1016/j.asr.2014.09.006.

Kaula, WM (1966). *Theory of satellite geodesy: applications of satellites to geodesy*. Courier Dover Publications.

Kleinherenbrink, M, Ditmar, PG and Lindenbergh, RC (2014). Retracking CryoSat data in the SARIn mode and robust lake level extraction. *Remote Sensing of Environment*, **152**(0):38–50. doi:10.1016/j.rse.2014.05.014.

Kleusberg, A and Wild-Pfeiffer, F (2008). Remote Sensing. *Lecture Note, Stuttgart University*.

Lee, H, Durand, M, Jung, HC, Alsdorf, D et al. (2010). Characterization of surface water storage changes in arctic lakes using simulated SWOT measurements. *International Journal of Remote Sensing*, **31**(14):3931–3953. doi:10.1080/01431161.2010.483494.

Lee, H, Shum, CK, Tseng, KH, Jun, YG et al. (2011). Present-day lake level variation from Envisat altimetry over the Northeastern Qinghai-Tibetan Plateau: links with precipitation and temperature. *Terrestrial, Atmospheric and Oceanic Sciences*, **22**(2):169–175. doi: 141.58.124.38.

Martin, TV, Zwally, HJ, Brenner, AC and Bindschadler, RA (1983). Analysis and retracking of continental ice sheet radar altimeter waveforms. *Journal of Geophysical Research: Oceans*, **88**(C3):1608–1616. doi:10.1029/JC088iC03p01608.

Morris, CS and Gill, SK (1994). Evaluation of the topex/poseidon altimeter system over the great lakes. *J Geophys Res*, **99**(C12):24,527–24,539. doi:10.1029/94JC01642.

Partington, KC, Ridley, JK, Rapley, CG and Zwally, HJ (1989). Observations of the surface properties of the ice sheets by satellite radar altimetry. *J Glaciol*, **35**(120):267–275.

Pengra, B, Chander, A, Litswa, E, Giese, K et al. (2012). The drying of Iran's lake Urmia and its environmental consequences. *UNEP-GRID, Sioux Falls, UNEP Global Environmental Alert Service (GEAS)*.

Rezvantalab, S and Amrollahi, MH (2011). Investigation of recent changes in Urmia salt lake. *International Journal)*, **2**(3).

Rosmorduc, V, Benveniste, J, Bronner, E, Dinardo, S et al. (2011). *Radar altimetry tutorial*. ESA and CNES.

Santos, SJ, Calmant, S, Seyler, F, Rotunno, FOC et al. (2010). Water levels in the Amazon basin derived from the ERS-2 and Envisat radar altimetry missions. *Remote Sensing of Environment*, **114**(10):2160–2181. doi:10.1016/j.rse.2010.04.020.

Shiklomanov, AI, Lammers, RB and Vörösmarty, CJ (2002). Widespread decline in hydrological monitoring threatens Pan-Arctic research. *Eos, Transactions American Geophysical Union*, **83**(2):13–17. doi:10.1029/2002EO000007.

Tourian, MJ, Elmi, O, Chen, Q, Devaraju, B et al. (2015). A spaceborne multisensor approach to monitor the desiccation of lake urmia in iran. *Remote Sensing of Environment*, **156**(0):349–360. doi:10.1016/j.rse.2014.10.006.

Tseng, KH, Shum, CK, Yi, YC, Fok, HS et al. (2013). Envisat altimetry radar waveform retracking of quasi-specular echoes over the ice-covered Qinghai lake. *Terrestrial, Atmospheric and Oceanic Sciences*, **24**(4I):615–627. doi:10.3319/TAO.2012.12.03.01(TibXS).

Vignudelli, S, Kostianoy, AG, Cipollini, P and Benveniste, J (2011). *Coastal altimetry*. Springer-Verlag Berlin Heidelberg. doi:10.1007/978-3-642-12796-0.

Wingham, D, Rapley, C and Griffiths, H (1986). New techniques in satellite altimeter tracking systems. *ESA Proceedings of the 1986 International Geoscience and Remote Sensing Symposium(IGARSS'86) on Remote Sensing: Today's Solutions for Tomorrow's Information Needs,*, **3**.

Yang, Y, Hwang, CW, Hsu, HJ, Dongchen, E et al. (2012). A subwaveform threshold retracker for ERS-1 altimetry: A case study in the Antarctic ocean. *Computers Geosciences*, **41**(0):88–98. doi:10.1016/j.cageo.2011.08.017.